

Orthorhombic Phase of Crystalline Polyethylene: A Monte Carlo Study

R. Martoňák^(1,2,*), W. Paul⁽¹⁾, K. Binder⁽¹⁾

⁽¹⁾ *Institut für Physik, KoMa 331, Johannes Gutenberg–Universität*

Staudingerweg 7, 55099 Mainz, Germany

⁽²⁾ *Max–Planck–Institut für Polymerforschung*

Ackermannweg 10, 55021 Mainz, Germany

(29 November 1996)

Abstract

In this paper we present a classical Monte Carlo simulation of the orthorhombic phase of crystalline polyethylene, using an explicit atom force field with unconstrained bond lengths and angles and periodic boundary conditions. We used a recently developed algorithm which apart from standard Metropolis local moves employs also global moves consisting of displacements of the center of mass of the whole chains in all three spatial directions as well as rotations of the chains around an axis parallel to the crystallographic *c*-direction. Our simulations are performed in the *NpT* ensemble, at zero pressure, and extend over the whole range of temperatures in which the orthorhombic phase is experimentally known to be stable (10 – 450 K). In order to investigate the finite-size effects in this extremely anisotropic crystal, we used different system sizes and different chain lengths, ranging from C₁₂ to C₉₆ chains, the total number of atoms in the super-cell being between 432 and 3456. We show here the results for structural parameters, such as the orthorhombic cell parameters *a*, *b*, *c*, and the setting angle of the chains, as well as internal parameters of the chains, such as the bond lengths and angles. Among ther-

mododynamic quantities, we present results for thermal expansion coefficients, elastic constants and specific heat. We discuss the temperature dependence of the measured quantities as well as the related finite-size effects. In case of lattice parameters and thermal expansion coefficients, we compare our results to those obtained from other theoretical approaches as well as to some available experimental data. We also suggest some possible ways of extending this study.

I. INTRODUCTION

Macromolecular crystals represent at the same time a particular case of a solid state system as well as that of a polymer system. The simplest and paradigmatic case in this field is crystalline polyethylene. As is well known, it is very difficult to obtain reliable experimental data for these systems, mainly due to problems associated with preparing sufficiently large monocrystalline samples. This increases the value of theoretical insight for understanding and eventual prediction of their properties. However, compared to the case of liquid polymer phases, a quantitative description of structure and properties of a solid phase is a more subtle problem. While in the former case it is often possible to replace whole monomer groups by united atoms and constrain the bond lengths and sometimes even the bond angles, in case of macromolecular crystals, instead, it is preferred to employ a force field for all atoms, without enforcing any constraints on the degrees of freedom [1].

Apart from the study of the ground state crystal structure and properties, which can be readily done within the framework of molecular mechanics, once a force field is available, the main interest lies in the finite temperature properties. At low temperatures, where the creation of conformational defects is unlikely, and the displacements of the atoms are relatively small, the structure of the PE crystal is dominantly governed by packing energetics of all-trans conformation chains. In this regime, phonon modes are well defined excitations of the system, and a possible theoretical approach is the use of quasi-harmonic or self-consistent quasi-harmonic approximations, which have the advantage of allowing for quantum effects to be taken into account easily [2–4].

Such methods are, however, intrinsically incapable of treating correctly the large amplitude, anharmonic motion of whole chain segments, which arises as the temperature approaches the melting point (at normal pressure about 414 K for a PE crystal). Actually, for crystalline PE they start to fail just at the room temperature of 300 K [4]. If the melting is prevented by increasing the external pressure, the orthorhombic crystal structure may persist to higher temperatures, and eventually undergo a phase transition into the hexagonal

”condis” phase, characterized by a large population of gauche defects [5]. In order to study the complex behavior in this high temperature regime, computer simulation techniques, like molecular dynamics or Monte Carlo, appear as a particularly convenient tool. Using a suitable ensemble and an appropriate simulation technique one can evaluate various thermodynamic quantities, like specific heat, elastic constants or thermal expansion coefficients, and structural quantities, such as bond lengths and angles, or defect concentration. It is also possible to directly study a variety of physically interesting phenomena associated with the structural phase transitions between different crystal modifications.

Computer simulations are, however, still limited to relatively small systems. In case of macromolecular crystals, the situation is rather peculiar due to the extreme anisotropy of the system originating from its quasi-one-dimensional character. When the chains are short, the system crosses over from a PE crystal to an *n*-paraffin crystal, which behaves in a substantially different way. Due to an easy activation of chain rotation and diffusion, *n*-paraffin crystals undergo, as the temperature is increased, a characteristic series of phase transitions, depending on the chain length (”rotator phases”, [6,7]). This fact makes it necessary to study and understand the related finite-size effects, if the results of the simulation are to be regarded as representative for the limit of very long chains, corresponding to PE, and interpreted in a consistent way. The choice of boundary conditions also represents a non-trivial issue, as documented by the very extensive explicit atom MD simulation [1], in which a transition from an initial orthorhombic structure to a parallel zig-zag chain arrangement was observed already at 111 K, contrary to experiment, probably because of the use of free boundary conditions in all spatial directions and a related large surface effect.

Finite temperature simulations of realistic, explicit atom models of crystals with long methylene chains, of which we are aware so far, have exclusively used molecular dynamics as the sampling method. Ryckaert and Klein [7] used a version of the Parrinello-Rahman MD technique with variable cell shape to simulate an *n*-paraffin crystal with constrained bond lengths and periodic boundary conditions. Sumpter, Noid, Liang and Wunderlich have simulated large crystallites consisting of up to 10^4 CH₂ groups, using free boundary

conditions [1]. Recently, Gusev, Zehnder and Suter [8] have simulated PE crystal using periodic boundary conditions, at zero pressure, using also the Parrinello-Rahman technique.

On the other hand, not much MC work seems to exist in this field, and to our knowledge, the only work is that of Yamamoto [9] which was aimed specifically at the high temperature "rotator" phases of *n*-paraffins. It concentrated exclusively on the degrees of freedom associated with the packing of whole chains, assumed to be rigid, neglecting completely the internal, intramolecular degrees of freedom.

The aim of this paper is twofold. On the one hand, we would like to explore the applicability of the MC method to a classical simulation of a realistic model of a PE crystal, using an explicit atom force field without any constraints, and periodic boundary conditions in all spatial directions. In order to have a direct access to quantities like thermal expansion coefficients, or elastic constants, we choose to work at constant pressure. If MC turns out to be a well applicable method for this system on the classical level, it would be a promising sign for an eventual Path Integral Monte Carlo (PIMC) study allowing to take into account also the quantum effects, known to play a crucial role at low temperatures [2–4]. It is known that for path integral techniques the use of MC is generally preferred to MD, because of the problem of non-ergodicity of the pseudo-classical system representing the quantum one in a path integral scheme. As a related problem, we would also like to understand the finite-size effects and determine for each particular temperature the minimal size of the system that has to be simulated in order to be reasonably representative of the classical PE crystal. Such information would also be very useful for an eventual PIMC study, where an additional finite-size scaling has to be performed, because of the finite Trotter number. On the other hand, we would like to study the physics of the orthorhombic phase of PE crystal in the classical limit over the whole temperature range of its experimentally known existence at normal pressure. We stress that our goal here is not to tune the force field in order to improve the agreement between the simulation and experiment. Our emphasis rather lies on providing results calculated for a given force field with an essentially exact classical technique. These might in future serve as a basis for estimation of the true importance of

quantum effects, when these can be taken into account by a PIMC technique, as well as for an assessment of the range of validity of different classical and quantum approximation schemes. Some preliminary simulation results of this study have been presented briefly in recent conference proceedings [10].

The paper is organized as follows. In Sect. II, we describe the force field as well as the constant pressure simulation method used. The MC algorithm itself will be addressed only briefly, since it has already been discussed in detail in its constant volume version in Refs. [11,10]. In Sect. III, we present the results for the structural and thermodynamic properties of the orthorhombic PE crystal obtained from zero pressure simulation in the temperature range 10 – 450 K, for different chain lengths and system sizes. We discuss the temperature dependence of the measured quantities as well as the related finite-size effects, and compare our results to those obtained from other theoretical approaches, as well as to some available experimental data. In the final Sect. IV we then draw conclusions and suggest some possible further directions.

II. CONSTANT PRESSURE SIMULATION METHOD

In this section we describe some details of the simulation method, as well as of the force field used. Before doing so, we recall here the structure of the orthorhombic PE crystal [12]. The unit cell contains two chains, each consisting of 2 CH_2 groups, giving a total of 12 atoms per unit cell. The all-trans chains extend along the crystallographic c -direction (z -axis) and are packed in a "herringbone" arrangement, characterized by the setting angle ψ (angle between the xz plane and the plane containing the carbon backbone of a chain) alternating from one raw of chains to another between the values $\pm|\psi|$. The packing is completely determined by specifying the 3 lattice parameters a, b, c as well as the value of $|\psi|$. To specify the internal structure of the chains, three additional parameters are needed, which may be taken to be the bond lengths r_{CH} and r_{CC} and the angle θ_{HCH} .

We have simulated a super-cell containing $i \times j \times k$ unit cells of the crystal, i, j, k being

integers. Periodic boundary conditions were applied in all three spatial directions, in order to avoid surface effects. Our PE chains with backbones consisting of $2k$ carbon atoms are thus periodically continued beyond the simulation box and do not have any chain ends.

As the study was aimed specifically at the orthorhombic phase of the PE crystal and we did not expect phase transitions into different crystal structures, we did not consider general fluctuations of the super-cell shape, otherwise common in the Parrinello - Rahman MD method. We have constrained the crystal structure angles α, β, γ to the right angle value, not allowing for shear fluctuations. The volume moves employed thus consisted only of an anisotropic rescaling of the linear dimensions of the system by three scaling factors s_1, s_2, s_3 , which relate the instantaneous size of the super-cell to that of the reference one. The reference super-cell always corresponded to lattice parameters $a = 7.25\text{\AA}$, $b = 5.00\text{\AA}$, $c = 2.53\text{\AA}$. The acceptance criterion for the volume moves was based on the Boltzmann factor $(s_1 s_2 s_3)^N e^{-\beta H}$, where $H = U + pV_0 s_1 s_2 s_3$, U is the potential energy of the system, p is the external pressure, V_0 the volume of the reference super-cell, and N the total number of atoms in the system. Throughout all simulations described in this paper, the external pressure was set to zero.

We come now to the description of the potential. We have used the force field developed for the PE crystal by Sorensen, Liau, Kesner and Boyd [13], with several slight modifications of the bonded interaction. This consists of diagonal terms corresponding to bond stretching, angle bending, and torsions, as well as of off-diagonal bond-bond, bond-angle and various angle-angle terms. For convenience, we have changed the form of the expansion in bond angles, replacing the expressions $(\theta - \theta_0)$ in all terms by $(\cos \theta - \cos \theta_0)/(-\sin \theta_0)$. The original form of the vicinal bend-bend interaction, having two different force constants, k_T and k_G for torsional angles close to trans and gauche minima, respectively, is useful for ground state studies, but not for a finite-temperature simulation, where the torsional angles may continuously fluctuate from one minimum to another. The form of this interaction has therefore been changed into the one used in Ref. [14], $k \cos \varphi (\cos \theta_1 - \cos \theta_0)(\cos \theta_2 - \cos \theta_0)$, where θ_1, θ_2 are bond angles, φ is a torsional angle, and k is a new force constant. The value

of the latter constant was taken to be $-k_T / \sin^2 \theta_0$ for C-C-C-C torsions and $2k_G / \sin^2 \theta_0$ for C-C-C-H torsions, in order to reproduce the curvature of the potential in the vicinity of the ground state equilibrium value of each torsional angle in the PE crystal. For H-C-C-H torsions, which are in the ground state in both trans and gauche minima, we took for k an approximate value of $k = (\sqrt{k_G k_T / \cos \frac{\pi}{3} \cos \pi}) / \sin^2 \theta_0$, which guarantees that both original force constants k_T and k_G are approximated in the vicinity of the respective minimum with the same error of about 8 %. At this point we comment on the torsional potential used. As the force field [13] has been originally designed for ground-state studies, the explicit torsional potential for all torsions contains only the term $\cos 3\varphi$, which yields zero energy difference between the trans and gauche minima in C-C-C-C torsions. The actual difference thus comes just from the non-bonded interaction superposed over 1 – 4 atoms, and is, according to Ref. [15], about 340 K, which is a somewhat higher value than the generally accepted one of about 250 K. However, the use of periodic boundary conditions anyway inhibits the creation of conformational defects strongly, and therefore this difference is not likely to play an important role, at least in the temperature range studied.

Concerning the nonbonded interaction, we used a spherical cutoff of 6 Å for all pair interactions, which corresponded to interaction of a given atom with about 110 neighbors. The list of neighbors has been determined at the beginning of the simulation with respect to the reference structure, and kept fixed throughout the evolution of the system (topological interaction). The use of the topological interaction would clearly preclude the longitudinal diffusion of the chains by creating an artificial energy barrier, which might be unrealistic for a study of short alkanes. However, since our main interest lies in the limit of very long chains, this approximation, common in the study of crystals, is acceptable here, and brings an advantage of considerably speeding up the execution of the program. The reference structure was obtained by placing the ideal crystal structure, described at the beginning of this section, inside the reference box, taking for the setting angle $|\psi|$ and the internal chain parameters the values of $|\psi| = 43.0^\circ$, $r_{CC} = 1.536 \text{ \AA}$, $r_{CH} = 1.09 \text{ \AA}$, $\theta_{HCH} = 107.4^\circ$, respectively. These values turned out to be to a good approximation close to their true average values throughout

the whole temperature range of the simulation, thus proving the consistency. Because of the relatively low cutoff used, we have added the long-range corrections to the non-bonded energy and diagonal components of the pressure tensor. These corrections have been calculated for the reference structure in the static lattice approximation, and tabulated for a suitable mesh of scaling factors s_1, s_2, s_3 . During the simulation, the values of the corrections corresponding to the instantaneous values of the scaling factors were calculated from the table by means of three-dimensional linear interpolation. We note here that our way of treating the non-bonded interaction is different from that used in [13], where the interaction of a given atom with two neighboring shells of chains has been taken into account and no long-range corrections have been applied.

The MC sampling algorithm for PE crystal was described in considerable detail in our previous papers [11,10], and here we present it just briefly. In addition to the volume moves, we used local moves to move the atoms and global moves to move the chains. In the local moves, the atoms of the crystal lattice were visited in sequential order, and different maximum displacements have been used for the atoms of carbon and hydrogen, reflecting the fact that a carbon atom has four covalent bonds while a hydrogen atom has just one. The typical value of the acceptance ratio for the local moves was kept close to 0.3, corresponding at temperature $T = 100$ K to isotropic maximum displacements of 0.03 \AA and 0.06 \AA for carbons and hydrogens, respectively. In the global moves, displacements of the center of mass of a whole chain along all three axes accompanied by rotation of the chain along a line parallel to the crystallographic c -direction and passing through the center of mass of the chain were attempted. Choosing the fraction of global moves to be 30 % in this study, the global and local moves were alternated at random, in order to satisfy the detailed balance condition. Once it was decided to perform a global move, all the chains of the super-cell were attempted to move in sequential order. For C_{12} chains at $T = 100$ K, the maximum (anisotropic) displacements of the chains were $\Delta x_{max} = \Delta y_{max} = 0.11 \text{ \AA}$, $\Delta z_{max} = 0.05 \text{ \AA}$, the maximum rotation angle being $\Delta\psi_{max} = 11^\circ$. This choice of the parameters resulted in an acceptance ratio of about 0.18 for the global moves. We note here that the energy change

associated with a rigid displacement or a rotation of a whole chain scales linearly with the length of the chain, and therefore for longer chains we reduced appropriately the parameters of the global moves in order to preserve the same acceptance ratio. No attempt to optimize the maximal displacements or fraction of different kinds of moves has been done in this study. Concerning the volume moves, we attempted a change of all three scaling factors s_1, s_2, s_3 after each sweep over the lattice (MCS) performing local or global moves. For the super-cell $2 \times 3 \times 6$ unit cells at $T = 100$ K, the maximum changes of the scaling factors used were $\delta s_1 = \delta s_2 = 0.0045, \delta s_3 = 0.0009$, where the different values reflected the anisotropy of the diagonal elastic constants c_{11}, c_{22}, c_{33} . This choice resulted in an acceptance ratio of 0.21 for the volume moves.

We have simulated several different super-cell sizes. The smallest one consisted of $2 \times 3 \times 6$ unit cells, contained 12 C₁₂ chains with a total of 432 atoms, and was used for simulation of the system at seven different temperatures ranging from 10 to 300 K. To study chain-length-dependent finite-size effects, at $T = 100$ K and $T = 300$ K the simulation was performed also on super-cells consisting of 12 C₂₄ and C₄₈ chains, containing respectively $2 \times 3 \times 12$ and $2 \times 3 \times 24$ unit cells, while at $T = 200$ K only the latter system size was studied in addition to the smallest one. At $T = 300$ K, a super-cell size $4 \times 6 \times 12$ unit cells, twice as large as the smallest one in each spatial direction, was also used, to study volume-related finite-size effects. Finally, at all four highest temperatures, $T = 300, 350, 400, 450$ K, a super-cell with the longest, C₉₆ chains was used, consisting of $2 \times 3 \times 48$ unit cells and containing 3456 atoms.

As the initial configuration for the lowest temperature simulation for a given super-cell size we used the corresponding reference structure. In course of the simulation, we made use of the final configuration of the run at a lower temperature when possible, and always equilibrated the system for at least 2×10^4 MCS before averaging. Our statistics is based on the run length of 1.4×10^6 MCS per data point for the smallest, 432 atom system, and a run length decreasing linearly with the number of atoms for the larger systems.

We have calculated the specific heat at constant pressure c_p from the enthalpy fluctua-

tions. The pressure tensor was calculated by means of a standard virial expression. In order to check the consistency of the simulation algorithm, we also evaluated the kinetic energy from the corresponding virial expression. During the averaging, the accumulators for the total energy, lattice parameters a, b, c and setting angle ψ were updated after each MCS while those for virial and other quantities were updated only every 10 MCS. Histograms have been accumulated for the structural quantities, like the bond lengths and angles, torsional angles and the setting angle of the chains as well as the displacement of the center of mass of the chains along the z -axis. The whole run was always subdivided into four batches and the batch subaverages were used to estimate the approximate error bars of the total averages.

Concerning the elastic constants $c_{11}, c_{22}, c_{33}, c_{12}, c_{13}, c_{23}$ (in the Voigt's notation), we have independently determined them in two different ways. Apart from the standard Parrinello-Rahman fluctuation formula [16]

$$c_{ik} = \frac{k_B T}{\langle V \rangle} \langle e_i e_k \rangle^{-1}, \quad i, k = 1, 2, 3, \quad (1)$$

we applied also the new fluctuation formula proposed in Ref. [17], in its approximate version suitable for small strain fluctuations

$$c_{ik} = - \sum_n \langle p_i e_n \rangle \langle e_n e_k \rangle^{-1}, \quad (2)$$

where p_i and e_i are the diagonal components of the pressure tensor and strain tensor, respectively.

III. RESULTS AND DISCUSSION

In this section we describe and discuss the results of the simulation. We start with a comment on the stability of the crystal structure. The initial structure with the characteristic "herringbone" arrangement of the chains was found to be stable at all temperatures and all system sizes except for the smallest system with C_{12} chains, where an occasional rotation of a whole chain was observed at $T = 300$ K. In the largest system with C_{96} chains, no

change of structure was observed up to $T = 450$ K. Although the latter temperature is larger than the experimentally known melting temperature of PE crystal (414 K), the use of periodic boundary conditions inhibits the melting and allows the simulation of a superheated crystalline phase. On the other hand, our arrangement with constrained angles of the supercell is compatible both with the orthorhombic and with the hexagonal phase, and would not prevent the system from entering the latter, which would occur when the ratio of the lattice parameters $\frac{a}{b}$ reaches the value $\sqrt{3}$. Our observation thus agrees with the experimentally known stability of the orthorhombic structure up to the melting point. In order to appreciate the amount of disorder present in the system at $T = 400$ K, we show in Fig.1 (a) a projection of the atoms on the xy plane for a typical configuration. The "herringbone" arrangement of the chains is still clearly visible, in spite of a well pronounced disorder. In Fig.1 (b), a projection of the same configuration on the xz plane is shown.

In Figs.2,3,4 we show the temperature dependence of the lattice parameters a, b, c . Extrapolating these curves down to $T = 0$, we find the ground state values of $a = 7.06\text{\AA}$, $b = 4.89\text{\AA}$, $c = 2.530\text{\AA}$. We note here that these values do not quite agree with those reported in Ref. [13], where the following values have been found $a = 7.05\text{\AA}$, $b = 4.94\text{\AA}$, $c = 2.544\text{\AA}$. We attribute these discrepancies to the different way of treating the non-bonded interaction as well as to our slight modifications of the bonded interaction.

Before discussing the thermal expansion of the lattice parameters, we comment on the finite-size effects observed. A particularly pronounced one is observed on the lattice parameter b , where the values for the smallest system with C_{12} chains are already at $T = 100$ K slightly larger than those for both systems with longer chains. The effect becomes stronger with increasing temperature. At $T = 300$ K, where we have data for four different chain lengths, the value of b is clearly seen to increase with decreasing chain length, most dramatically for the system with C_{12} chains. On the other hand, a considerably weaker finite-size effect is seen on lattice parameters a and c . While for the latter one it is perhaps not surprising, because of the large stiffness of the system in the chain direction, the distinct behavior of the b parameter with respect to the a parameter does not appear to be so

straightforward to interpret. We believe that its origin lies in the particular character of the chain packing, where the shortest hydrogen-hydrogen contact distance is just that along the crystallographic b -direction (y -axis) [18]. This results in a stronger coupling of the lateral strain ϵ_2 along the b -direction to the longitudinal displacements of whole chains. Since the fluctuations of these displacements are larger for systems with short chains, a particular finite-size effect arises.

Concerning the thermal expansion itself, it is convenient to discuss separately the case of the lateral lattice parameters a, b , and that of the axial one c . We start with the lateral ones, and show in Fig.5 also the temperature dependence of the aspect ratio $\frac{a}{b}$. Two regimes can be clearly distinguished here. For temperatures up to about 250 K, both lattice parameters expand in a roughly linear way with increasing temperature, and the ratio $\frac{a}{b}$ raises only slightly from its ground state value of 1.44 (which differs substantially from the value of $\sqrt{3} = 1.73$, corresponding to hexagonal structure). It is characteristic for this regime that the thermal expansion arising due to lattice anharmonicities can be described within a *phonon picture* using a quasi-harmonic or self-consistent quasi-harmonic approximation [2–4]. For higher temperatures, the picture changes. While the lattice parameter a starts to increase faster, the expansion of the parameter b at the same time becomes more slow until it develops a maximum at $T = 350$ K, where it starts to decrease again. Such behavior of b has been already observed in the work [7]. As a consequence, the aspect ratio $\frac{a}{b}$ increases strongly. This suggests that the driving force of the change of the lateral lattice parameters in this regime is the approach of a phase transition to a hexagonal phase, in which each chain is surrounded by six chains at equal distance. We have actually continued our simulations to even higher temperatures, and from a limited amount of simulation performed in that region we have found an indication that the hexagonal phase is indeed reached in the range of temperatures 500 – 550 K (Fig.5). It is, however, clear that in order to obtain reliable results from the simulations in this high-temperature range, where the phase transition in a real PE crystal involves large amplitude displacements and rotations of the whole chains, as well as a considerable population of conformational defects, it would be necessary to

introduce several modifications into the simulation algorithm. We shall come back to this point again in the final section.

In Fig.6, the temperature dependence of the average setting angle $\langle |\psi| \rangle$ of the chains is shown. It also fits well within the two regimes scenario, being rather flat up to $T = 300$ K, and then starting to decrease. This decrease could indicate an approach of the value of $|\psi| = 30^\circ$, compatible with the symmetry of the hexagonal phase. It is also interesting to note the pronounced finite-size effect, similar to that observed in the case of b .

Before discussing the temperature dependence of the axial lattice parameter c , it is convenient to plot also the thermal expansion coefficients, defined as $\alpha_i = a_i^{-1} da_i/dT, i = 1, 2, 3$, where a_1, a_2, a_3 are the lattice parameters a, b, c . These have been obtained by taking the finite differences of the lattice parameters and are shown in Figs.7,8,9 as a function of temperature. As their behavior trivially follows from that of the lattice parameters, discussed for $i = 1, 2$ above, we just note here that all three coefficients converge at low temperatures to nonzero finite values, as can be expected in the classical limit.

Concerning the behavior of c and α_3 , the characteristic feature is that α_3 is negative in the whole temperature range and an order of magnitude smaller than α_1 . It is interesting here to compare our result for α_3 to that found in Ref. [2] within the quasi-harmonic approximation for a different force field [14]. A distinct feature of the latter result is that the classical value of α_3 is considerably smaller in magnitude than the quantum mechanical value (and also the experimental one), and approaches zero as $T \rightarrow 0$. Since in the classical limit there is no a priori reason for such behavior, it has to be regarded as accidental. According to the argumentation in Ref. [2], there are contributions of different sign to α_3 from different phonon modes, negative from lattice modes (mainly backbone torsions), and positive from the harder ones. In the classical limit, all the modes contribute at all temperatures and happen to just cancel each other as $T \rightarrow 0$. In order to estimate the amount of contribution of the torsions in our case, we have made use of the work [3], where a formula is derived for the axial thermal contraction in a simple one-chain model with only torsional degrees of freedom. In

the classical limit, the formula predicts $c - c_0 = -\frac{1}{4}c_0 \sin^2 \frac{\alpha}{2} \langle \phi_{CCCC}^2 \rangle$, where $\alpha = \pi - \theta_{CCC}$, and ϕ_{CCCC} is the fluctuation of the torsional angle φ_{CCCC} from the trans minimum. In Fig.10 we have plotted c against $\langle \phi_{CCCC}^2 \rangle$, and found a very good linear dependence over the whole temperature range up to 450 K, where the effective torsional constant, defined as $C_{tors} = \frac{T}{\langle \phi_{CCCC}^2 \rangle}$, undergoes a considerable softening with increasing temperature (Fig.11). The proportionality constant determined from our plot was, however, larger in magnitude by about 50 % with respect to the above value of $\frac{1}{4}c_0 \sin^2 \frac{\alpha}{2}$, valid for the simple model. The linear dependence suggests that with the force field used [13], the negative α_3 originates almost entirely from the C-C-C-C torsions, which points to a certain intrinsic difference in the anharmonic properties of the force fields [13] and [14]. The pronounced increase of α_3 for $T > 300$ K is thus a consequence of a strong softening of the torsional potential due to the large amplitude of the fluctuations.

For comparison of these results to experimental ones, we have chosen two sets of data. In the work [19], lattice parameters a, b, c have been measured in the temperature range 93 – 333 K, and the data are smooth enough to allow a direct extraction of thermal expansion coefficients by means of finite differences. The other chosen set of data [20] is to our knowledge the only one covering the range from helium temperatures up to $T = 350$ K, however, the scatter of the data is too large for a direct numerical differentiation. Therefore we decided to first fit them by a fourth-order polynomial and then evaluate the expansion coefficients analytically. For both sets, the experimental values of the lattice parameters are shown in Figs.2,3,4 and the corresponding thermal expansion coefficients in Figs.7,8,9 .

Concerning the absolute value of the lattice parameters, in case of a our results agree well with the data [19], while falling slightly below the data [20], in particular at the lowest temperatures. In case of b our results fall slightly above and in that of c slightly below both data sets in the whole temperature range. As far as the temperature dependence itself is concerned, this is most conveniently discussed in terms of the thermal expansion coefficients α_i . We note first that for temperatures lower than about 150 K, quantum effects become crucial and cannot be neglected, as they are responsible for the vanishing of all

expansion coefficients in the limit $T \rightarrow 0$. A meaningful comparison of our classical results to experimental data is thus possible only for larger temperatures. For $T > 150$ K, α_1 agrees qualitatively well with the data [19], although the experimental ones appear to be slightly smaller. In particular, the pronounced increase of α_1 for $T > 250$ K appears to be well reproduced, in contrast to the result obtained in Ref. [2] within the classical quasi-harmonic approximation for the force field [14]. The agreement is less good for the data [20], which are distinctly smaller and start to increase strongly at somewhat smaller temperatures, for $T > 200$ K. In case of α_2 , our data agree for $T > 150$ K qualitatively well with the set [20], correctly reproducing the gradual decrease with temperature, although our results are somewhat smaller. The data [19] exhibit here a different behavior, being of the same magnitude as the ones in Ref. [20], but markedly flat in the whole range of temperatures. We note here that in the work [21], $\alpha_2 < 0$ has been experimentally observed just below the melting point. On the other hand, the classical result for α_2 calculated in Ref. [2] exhibits instead an upward curvature. Concerning α_3 , our results agree quantitatively well with the data [19] in the whole range of temperatures, although some scatter of the data precludes here a more detailed comparison. In the set [20], α_3 behaves for $T > 100$ K qualitatively similar to our results, however, the plateau value is somewhat smaller and the strong increase in magnitude appears at a lower temperature, already between 200 - 250 K. The origin of some of the observed discrepancies may be either in the force field itself, or in the quantum effects, which may be relevant even at temperatures as high as 300 K [2]. Also our fit of the data [20] is not unique, and may itself be a source of additional errors in the coefficients α_i . Last, but not least, it appears that there exists also a considerable scatter between the experimental data from different sources. We therefore believe that it would be interesting to re-examine the temperature dependence of the structural parameters (including possibly the setting angle of the chains) of well-crystalline samples of PE, in the whole range from very low temperatures up to the melting point, using up-to-date X-ray or neutron diffraction techniques.

In Fig.12, the average fluctuations $\sqrt{\langle(\delta|\psi|)^2\rangle}$ of the setting angle of the chains are shown as a function of temperature. Apart from a trivial finite-size effect of average fluctuation increasing with decreasing chain length, we note that for the system with C_{12} chains the curve exhibits a marked enhancement of the fluctuations at $T = 300$ K. Such enhancement suggests that the system is approaching a transition into a phase similar to the "rotator" phases of n -paraffins, where the setting angle of the chains jumps among several minima. For the system with C_{96} chains, the same phenomenon occurs only for $T > 400$ K, which in a real PE crystal coincides with the melting point. In Fig.13, we show a histogram of the setting angle ψ for the system with C_{96} chains at the highest temperature $T = 450$ K. The distribution is still bimodal, with two peaks centered at $\pm\langle|\psi|\rangle$, as it is in the ground state, corresponding to the "herringbone" arrangement of the chains. This proves that in our super-cell with periodic boundary conditions in all directions, the superheated orthorhombic structure is stable even at such high temperature, at least on the MC time scale of our run.

We comment now briefly on some other internal structural parameters. In Figs.14 and 15, we show the average angles $\langle\theta_{CCC}\rangle$ and $\langle\theta_{HCH}\rangle$ as a function of temperature. While the angle $\langle\theta_{CCC}\rangle$ develops between 250 and 300 K a very shallow minimum, the angle $\langle\theta_{HCH}\rangle$ decreases roughly linearly throughout the whole range of temperatures, its overall variation being about a factor of 3 larger than that of the former. Both average bond lengths $\langle r_{CC} \rangle$ and $\langle r_{CH} \rangle$ increase very slightly with temperature, the dependence being very close to linear, $\langle r_{CC} \rangle$ varying from 1.5357 Å at 10 K to 1.5398 Å at 450 K, and $\langle r_{CH} \rangle$ varying from 1.0898 Å at 10 K to 1.0924 Å at 450 K. It is interesting to show the average torsional fluctuations $\sqrt{\langle\phi_{CCCC}^2\rangle}$ as a function of temperature, Fig.16, where we see an enhancement for $T > 400$ K, corresponding to already discussed softening of the effective torsional potential (Fig.11). The typical fluctuation in this region is about 13°. From the histograms of the torsional angles we found that for temperatures up to 400 K, no gauche defects are created in the chains, while at 450 K only an extremely low population starts to arise. This is clearly a consequence of the periodic boundary conditions used in the chain direction together with

the still relatively short length of the chains used.

We come now to some thermodynamic parameters, and start with the specific heat per unit cell. This is shown in Fig.17 as a function of temperature. At low temperatures, where the classical crystal is always harmonic, $\frac{c_p}{k_B}$ reaches the classical equipartition value of 18, corresponding to $3 \times 12 = 36$ degrees of freedom per unit cell. With increasing temperature, as the anharmonicities become important, its value gradually increases, until a finite size effect starts to appear for $T > 200$ K. While for the system with C_{12} chains c_p starts to grow faster for $T > 200$ K, for the system with C_{96} chains this occurs only at about 300 K. This behavior is likely to be related to the already discussed chain-length-dependent onset of increased fluctuations of the setting angle, or rotations of the chains around their axes.

In Figs.18 – 22, we show the elastic constants $c_{11}, c_{22}, c_{12}, c_{13}, c_{23}$, determined by means of the Parrinello-Rahman fluctuation formula (1), as a function of temperature. For the case of c_{33} , we show in Fig.23 both the values obtained according to the Parrinello-Rahman fluctuation formula (1) and those found from the new formula (2). We see that the values obtained with the latter one have considerably smaller scatter. Actually, we have tried to use the formula (2) also for other elastic constants, however, only in the case of c_{33} a definite improvement of the convergence was observed. It would certainly be desirable to be able to improve on the accuracy of the elastic constants, in particular in case of c_{13}, c_{23} ; however, at present this seems to require a prohibitively large CPU time unless a considerably more efficient algorithm is available. At this point we note that some of the error bars shown in the figures for the elastic constants are probably an underestimate of the true ones, as they have been obtained from the variance of the results from just four batches.

To discuss now the temperature dependence of the elastic constants, it's again convenient to do so separately for the lateral ones c_{11}, c_{22}, c_{12} , and for the ones related to the axial strain ϵ_3 , namely c_{13}, c_{23}, c_{33} . All three constants c_{11}, c_{22}, c_{12} are seen to monotonously decrease with temperature, reaching at 400 K, just below the melting point, about 60 % or even less of their ground state values. This behavior originates mainly from the thermal expansion of the crystal in the lateral directions and is typical for van der Waals systems, like, e.g., solid

argon [22]. An interesting finite-size effect is seen on the diagonal elastic constant c_{22} , which is at $T = 300$ K distinctly smaller for the system with C_{12} chains than for other systems. This observation correlates with the effect seen on lattice parameter b , which was in turn found to be larger for the system with the shortest chains.

Concerning the other group of elastic constants, we first note that the diagonal one c_{33} is two orders of magnitude larger than all the other elastic constants. At low temperatures, c_{33} reaches a limiting value as large as 340 GPa and decreases monotonously with increasing temperature, dropping at 400 K to about 80 % of its ground state value. On the other hand, the two off-diagonal elastic constants, c_{13} and c_{23} , are, interestingly, found to increase with temperature, in agreement with the results in Ref. [2]. Taking into account the negative thermal expansion of the system in the axial direction, the behavior of this group of elastic constants does not appear to be just a trivial consequence of the thermal expansion, as it was in the case of c_{11}, c_{22}, c_{12} . In order to understand such behavior, it is interesting to plot also the elastic constant c_{33} vs. the mean-square fluctuation of the torsional angle $\langle \phi_{CCCC}^2 \rangle$, Fig.24. We find again a roughly linear dependence (compare Fig.10), which suggests that the softening of c_{33} is directly related to the activation of the torsional degrees of freedom. The mechanism underlying the behavior of these elastic constants then might be the following. At $T = 0$, where the chain backbones are perfectly flat in their all-trans states, an axial deformation can be accommodated only by bending the bond angles θ_{CCC} . Angle bending is, however, after bond stretching, the second most stiff degree of freedom in the system and determines the high ground state value of c_{33} . As the torsional fluctuations become activated with increasing temperature, the chains start to "wiggle" and develop transverse fluctuations (see Fig.1 (b)). In such configurations, it becomes possible to accommodate a part of the axial deformation in the torsional modes, which represent the most soft ones in the bonded interaction, and c_{33} is therefore renormalized to a smaller value. This must be, however, accompanied by an increased response of the transverse fluctuations of the chains, resulting in lateral strain, because of the "wiggling", since the total length of the chains is very hard to change. An increased lateral strain response to an axial strain means, however,

just an increase of the value of the elastic constants c_{13} and c_{23} . It would be, of course, desirable to have a quantitative theory supporting this intuitive, but, as we believe, well plausible interpretation.

The reason why the constants c_{13} and c_{23} appear to have the largest error bars among all elastic constants also seems to be connected with the fact that these two ones express just the coupling between the lateral and axial strains. The computational efficiency of the algorithm in determination of these two quantities is crucially dependent on the exchange of energy between the non-bonded and bonded interactions, which is probably still the most difficult point even with the present algorithm, because of the large separation of the relevant energy scales.

Before closing this section, we would like to make yet few more remarks on the finite-size effects. Comparing the results at $T = 300$ K for both systems consisting of C_{24} chains, containing respectively $2 \times 3 \times 12$ and $4 \times 6 \times 12$ unit cells, we see that the values obtained with both system sizes are for all quantities practically equal. This suggests that the finite-size effects related directly to the volume of the box are relatively small, at least for the two system sizes considered (which are, however, still not very large). On the other hand, a definite chain-length-dependent finite-size effect has been found in case of several quantities for the chain lengths considered, its magnitude being also distinctly temperature dependent. For practical purposes, it results that the smallest system size used with C_{12} chains can be representative of a classical PE crystal only at rather low temperatures, perhaps below 100 K, since at and above this temperature it exhibits pronounced finite-size effects. On the other hand, the systems with C_{24} and C_{48} chains appear to represent the classical PE crystal reasonably well for temperatures lower than 300 K, while at this and higher temperatures the use of a system with C_{96} chains or even longer would be strongly recommended.

IV. CONCLUSIONS

In this paper, we have demonstrated three main points. First, the MC algorithm using global moves on the chains in addition to the local moves on the atoms is a well applicable method for a classical simulation of crystalline PE. It allows an accurate determination of the structural properties and yields also fairly accurate results for the elastic constants. Second, the force field we have used [13] is well able to reproduce the experimentally known structure in the whole range of temperatures, and where the classical description is appropriate, the results obtained agree well with the available experimental data. Third, we have studied the finite-size effects, mainly due to chain length, and determined for different temperatures a minimal chain length necessary for the system to be in the limit of long chains, and thus representative of PE. All these findings look promising for further studies, and here we suggest some possible directions.

Basically, there are two routes to extend the present study, concentrating on the low-temperature and high-temperature region, respectively. The first one would aim on taking into account the quantum effects, e.g. by means of a Path Integral MC technique. Apart from improving the agreement with experiment, mainly at low temperatures, this technique is able to treat the quantum effects at a finite temperature in an essentially exact way and therefore should also allow to check the range of validity of various approximate treatments, like the quasi-harmonic or self-consistent quasi-harmonic approximations [2,3]. This would help to understand better the true importance of quantum effects at different temperatures in this paradigmatic crystalline polymer system.

The second route would aim on the high-temperature region of the phase diagram, where the orthorhombic crystal melts under normal pressure, but is known to undergo a phase transition into a hexagonal "condis" phase at elevated pressure [5]. In the present simulation arrangement, melting is prevented by periodic boundary conditions in both lateral directions, but the same boundary conditions being applied in the chain direction inhibit also the creation of conformational defects. Nevertheless, there are indications arising from the

present simulation that a similar transition could indeed occur in the temperature region 500 – 550 K, the main ones being the approach of the aspect ratio $\frac{a}{b}$ towards the hexagonal value of $\sqrt{3}$, and enhancement of the torsional angle and setting angle fluctuations for temperatures over 400 K. In order to study this high-temperature regime properly, several modifications of the present algorithm would be necessary. The main one would be a lifting of the periodic boundary conditions in the chain direction, thus introducing free chain ends. A use of a larger cutoff for the non-bonded interactions would be necessary in order to treat correctly the large amplitude displacements and rotations of the chains involved in the transition, and perhaps a non-spherical cutoff including certain number of atoms from one or two neighboring shells of chains around a given atom might be a preferred solution. It would also be necessary to modify the torsional potential in order to yield a correct value for the energy difference between the trans and gauche states. In order to be able to sample configurations with a considerable population of conformational defects, it might also be useful to introduce some other kind of MC moves acting on the torsional degrees of freedom. Finally, a full MC version of the Parrinello-Rahman variable-cell-shape technique should be introduced in order to allow also for shear fluctuations. These might in principle be substantially involved in the transition itself, although the hexagonal phase can be reached from the orthorhombic one without creating a static shear strain.

Before closing, we also emphasize that techniques similar to those applied here should be useful for a wide variety of other macromolecular crystals.

ACKNOWLEDGMENTS

We would like to acknowledge stimulating discussions with A. A. Gusev, P. C. Hägele, K. Kremer, R. J. Meier, A. Milchev, F. Müller-Plathe, M. Müser, P. Nielaba, G. C. Rutledge, G. Smith, U. W. Suter, E. Tosatti, M. M. Zehnder, as well as correspondence with R. H. Boyd and R. A. Stobbe.

REFERENCES

* Permanent address: Department of Physics, Faculty of Electrical Engineering, Slovak Technical University, Ilkovičova 3, 812 19 Bratislava, Slovakia.

- [1] G. L. Liang, D. W. Noid, B. G. Sumpter, B. Wunderlich, *Comp. Pol. Sci.* **3**, 101 (1993); B. G. Sumpter, D. W. Noid, G. L. Liang, B. Wunderlich in: *Atomistic Modeling of Physical Properties*, ed. by L. Monnerie, U. W. Suter, *Advances in Polymer Science*, 116 (Springer-Verlag, 1994), p. 27.
- [2] D. J. Lacks, G. C. Rutledge, *J. Phys. Chem.* **98**, 1222 (1994).
- [3] R. A. Stobbe, P. C. Hägele, *J. Polym. Sci., Part B, Polym. Phys.*, **34**, 975 (1996).
- [4] R. A. Stobbe, Ph.D. Thesis, Universität Ulm, Abteilung Angewandte Physik, 1996.
- [5] B. Wunderlich, M. Möller, J. Grebowicz, H. Baur, *Adv. Polym. Sci.* **87** (1988).
- [6] G. Ungar, *J. Phys. Chem.* **87**, 689 (1983).
- [7] J. P. Ryckaert, M. L. Klein, *J. Chem. Phys.* **85**, 1613 (1986).
- [8] A. A. Gusev, M. M. Zehnder, U. W. Suter in: W. L. Mattice, *Molecular Modeling of Polymers*, ACS Short Courses, 1996.
- [9] T. Yamamoto, *J. Chem. Phys.* **82**, 3790 (1985), *J. Chem. Phys.* **89**, 2356 (1988).
- [10] R. Martoňák, W. Paul, K. Binder, submitted to *J. Comp.-Aid. Mat. Des.*
- [11] R. Martoňák, W. Paul, K. Binder, to appear in *Comp. Phys. Comm.*
- [12] S. Kavesh, J. M. Schultz, *J. Polym. Sci., Part A-2*, **8**, 243 (1970).
- [13] R. A. Sorensen, W. B. Liau, L. Kesner and R. H. Boyd, *Macromolecules* **21**, 200 (1988).
- [14] N. Karasawa, S. Dasgupta, W. A. Goddard III, *J. Phys. Chem.* **95**, 2260 (1991).
- [15] R. H. Boyd, private communication.

- [16] M. Parrinello, A. Rahman, J. Chem. Phys. **76**, 2662 (1982).
- [17] A. A. Gusev, M. M. Zehnder, U. W. Suter, Phys. Rev. B **54**, 1 (1996).
- [18] B. Wunderlich, *Macromolecular Physics*, Vol. I; Academic Press: New York, 1973.
- [19] G. T. Davis, R. K. Eby, J. P. Colson, J. Appl. Phys. **41**, 4316 (1970).
- [20] G. Dadobaev, A. I. Slutsker, Sov. Phys. Solid State, **23**, 1131 (1981).
- [21] P. R. Swan, J. Polym. Sci., **56**, 403 (1962).
- [22] D. O. Löding, Diploma Thesis, Institut für Physik, Universität Mainz, 1996, p.35.

FIGURES

Fig.1. A snapshot of a projection of a typical configuration of the system at $T = 400$ K on the xy plane (a), and on the xz plane (b). The size of the reference super-cell is $L_x = 14.5\text{\AA}$, $L_y = 15.0\text{\AA}$, $L_z = 121.44\text{\AA}$. Filled points represent the carbon atoms, empty ones the hydrogen atoms. Note that the "herringbone" arrangement of the chains is still clearly visible in (a).

Fig.2. Temperature dependence of the lattice parameter a , shown for different system sizes, together with the experimental data [19,20]. In this and most of the following figures, statistical error bars are shown, lines are for visual help only.

Fig.3. Temperature dependence of the lattice parameter b , shown for different system sizes, together with the experimental data [19,20]. Note the finite-size effect.

Fig.4. Temperature dependence of the lattice parameter c , shown for different system sizes, together with the experimental data [19,20].

Fig.5. Temperature dependence of the aspect ratio $\frac{a}{b}$. Note the approach towards the hexagonal value of $\sqrt{3} = 1.732$ with increasing temperature.

Fig.6. Temperature dependence of the average setting angle $\langle|\psi|\rangle$ of the chains, shown for different system sizes. Note the finite-size effect.

Fig.7. Thermal expansion coefficient α_1 as a function of temperature, shown for different system sizes, together with the experimental data [19,20].

Fig.8. Thermal expansion coefficient α_2 as a function of temperature, shown for different system sizes, together with the experimental data [19,20]. Note the finite-size effect.

Fig.9. Thermal expansion coefficient α_3 as a function of temperature, shown for different system sizes, together with the experimental data [19,20].

Fig.10. Lattice parameter c vs. $\langle \phi_{CCCC}^2 \rangle$, shown for different system sizes. Note the linear dependence over the whole temperature range, which can be fitted by a line $c = 2.530 - 9.50 \times 10^{-5} \langle \phi_{CCCC}^2 \rangle$.

Fig.11. Temperature dependence of the effective torsional force constant $C_{tors} = \frac{T}{\langle \phi_{CCCC}^2 \rangle}$, shown for different system sizes. Note the considerable softening with increasing temperature.

Fig.12. Temperature dependence of the average fluctuation $\sqrt{\langle (\delta|\psi|)^2 \rangle}$ of the setting angle of the chains, shown for different system sizes.

Fig.13. Histogram of the setting angle ψ of the chains for the system with C_{96} chains at the highest temperature $T = 450$ K. Note that the distribution is still bimodal, corresponding to the "herringbone" arrangement of the chains.

Fig.14. Temperature dependence of the average bond angle $\langle \theta_{CCC} \rangle$, shown for different system sizes. Note the minimum at 300 K.

Fig.15. Temperature dependence of the average bond angle $\langle \theta_{HCH} \rangle$, shown for different system sizes.

Fig.16. Temperature dependence of the average fluctuation $\sqrt{\langle \phi_{CCCC}^2 \rangle}$ of the torsional angle φ_{CCCC} from the trans minimum, shown for different system sizes.

Fig.17. Temperature dependence of the specific heat per unit cell at constant pressure c_p , shown for different system sizes.

Fig.18. Elastic constant c_{11} as a function of temperature, shown for different system sizes.

Fig.19. Elastic constant c_{22} as a function of temperature, shown for different system sizes. Note the finite-size effect.

Fig.20. Elastic constant c_{12} as a function of temperature, shown for different system sizes.

Fig.21. Elastic constant c_{13} as a function of temperature, shown for different system sizes. Note the increase with temperature.

Fig.22. Elastic constant c_{23} as a function of temperature, shown for different system sizes. Note the increase with temperature.

Fig.23. Elastic constant c_{33} as a function of temperature, shown for different system sizes. Empty and filled symbols represent data determined from the formulas (1) and (2), respectively. Note the smaller scatter of the latter results.

Fig.24. Elastic constant c_{33} vs. $\langle \phi_{CCCC}^2 \rangle$, shown for different system sizes. Note the roughly linear dependence.

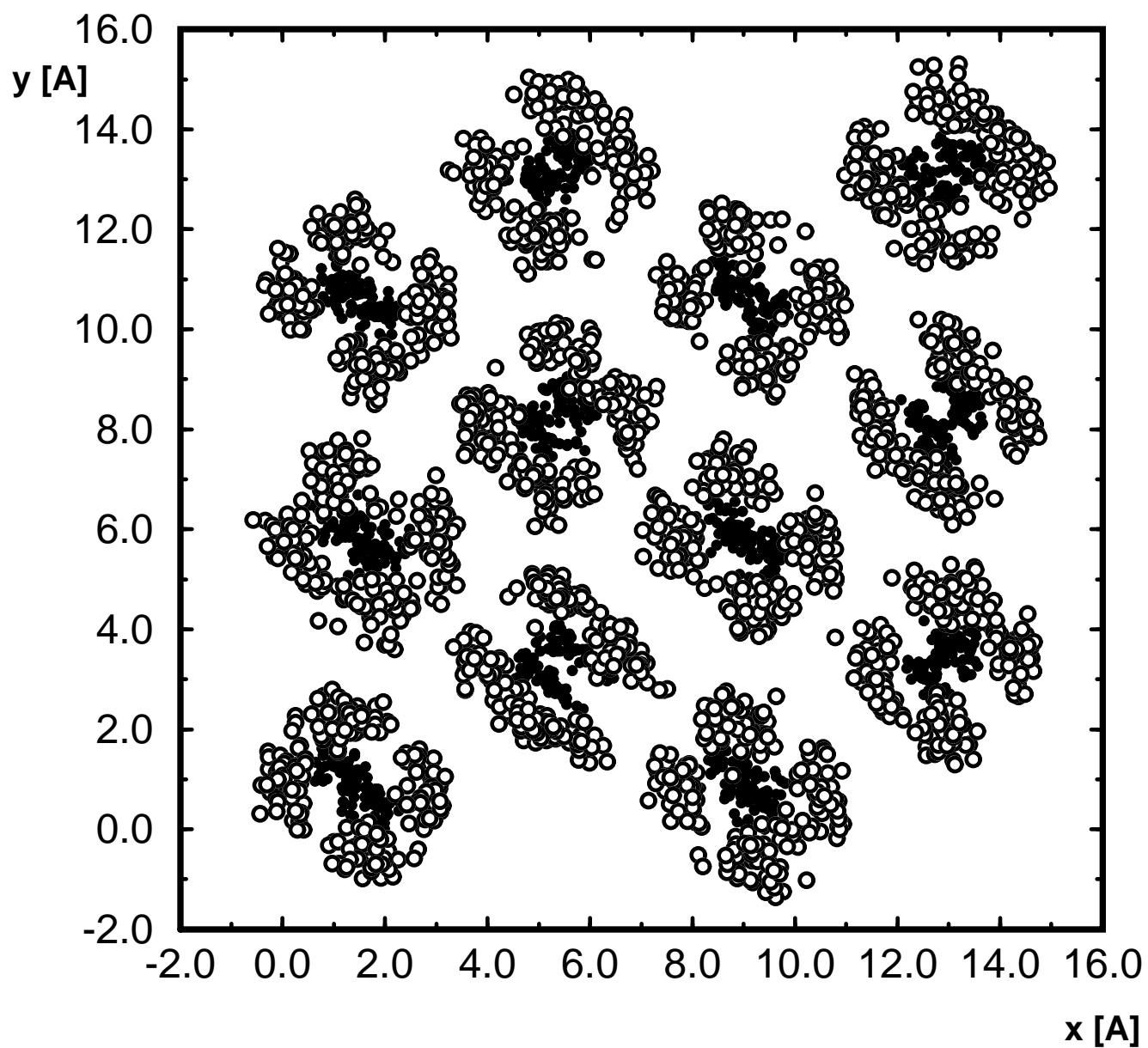


Fig.1(a) R. Martonak et al., J. Chem. Phys.

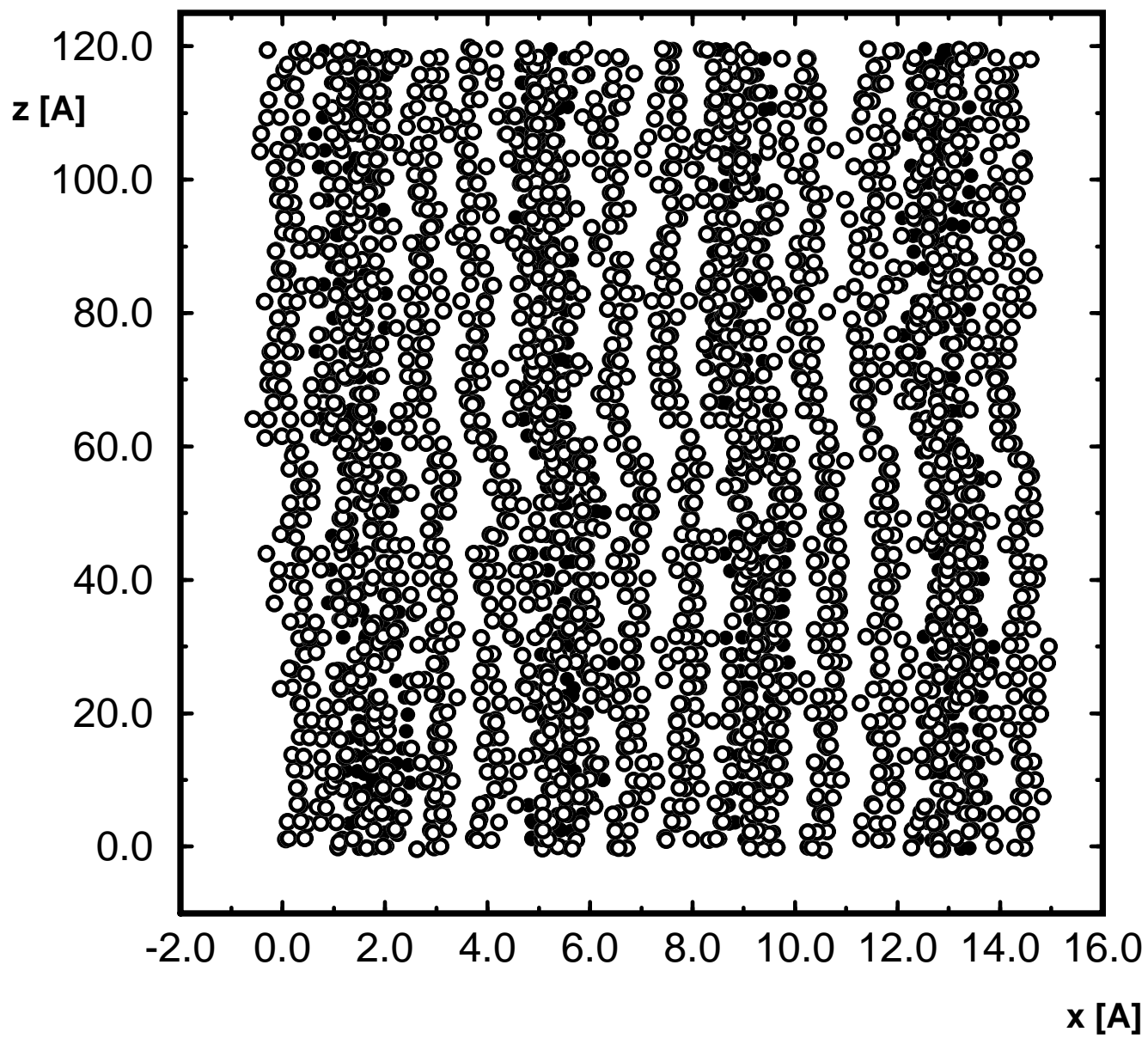


Fig.1 (b) R. Martonak et al., J. Chem. Phys.

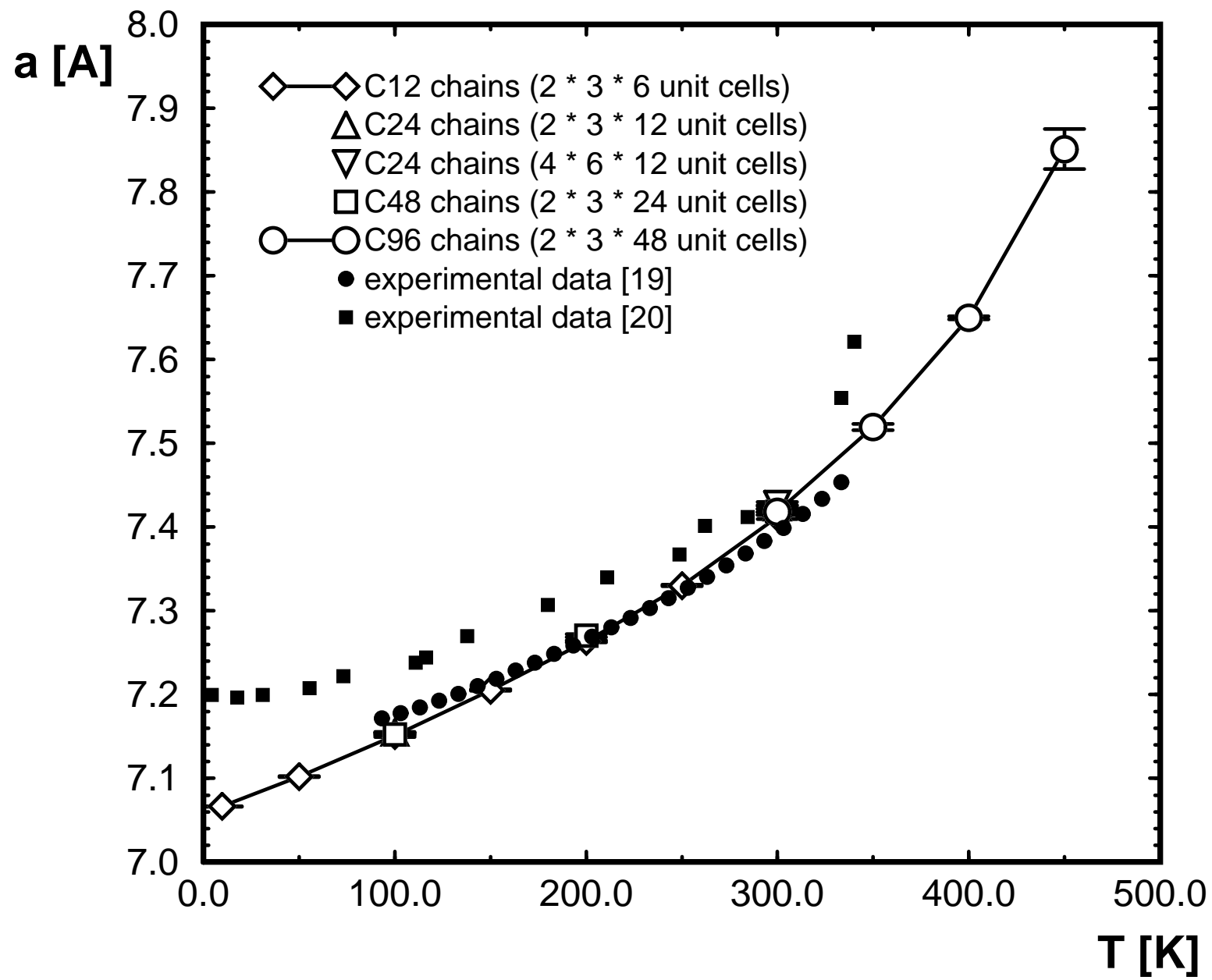


Fig. 2

R. Martonak et al., J. Chem. Phys.

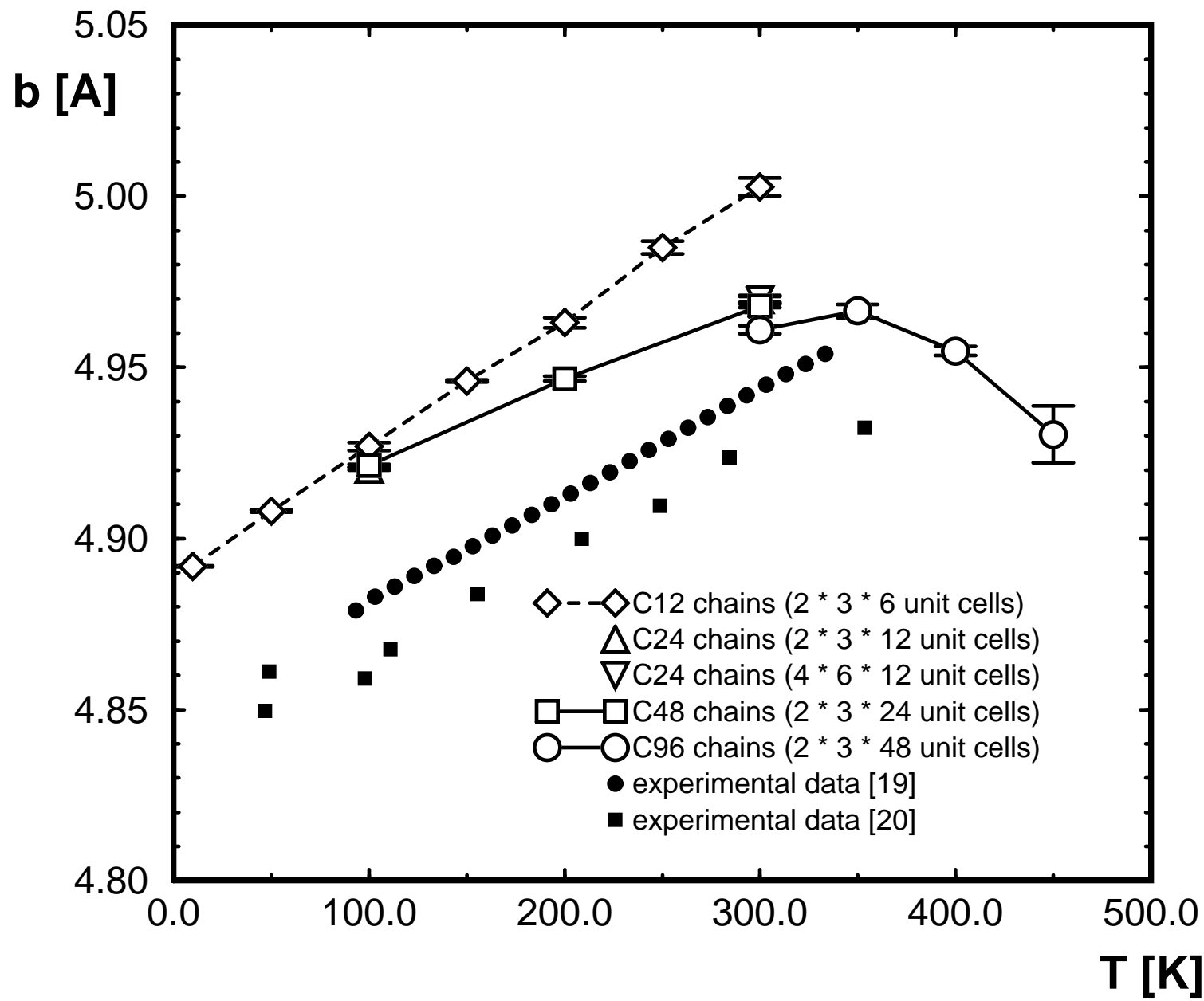


Fig. 3

R. Martonak et al., J. Chem. Phys.

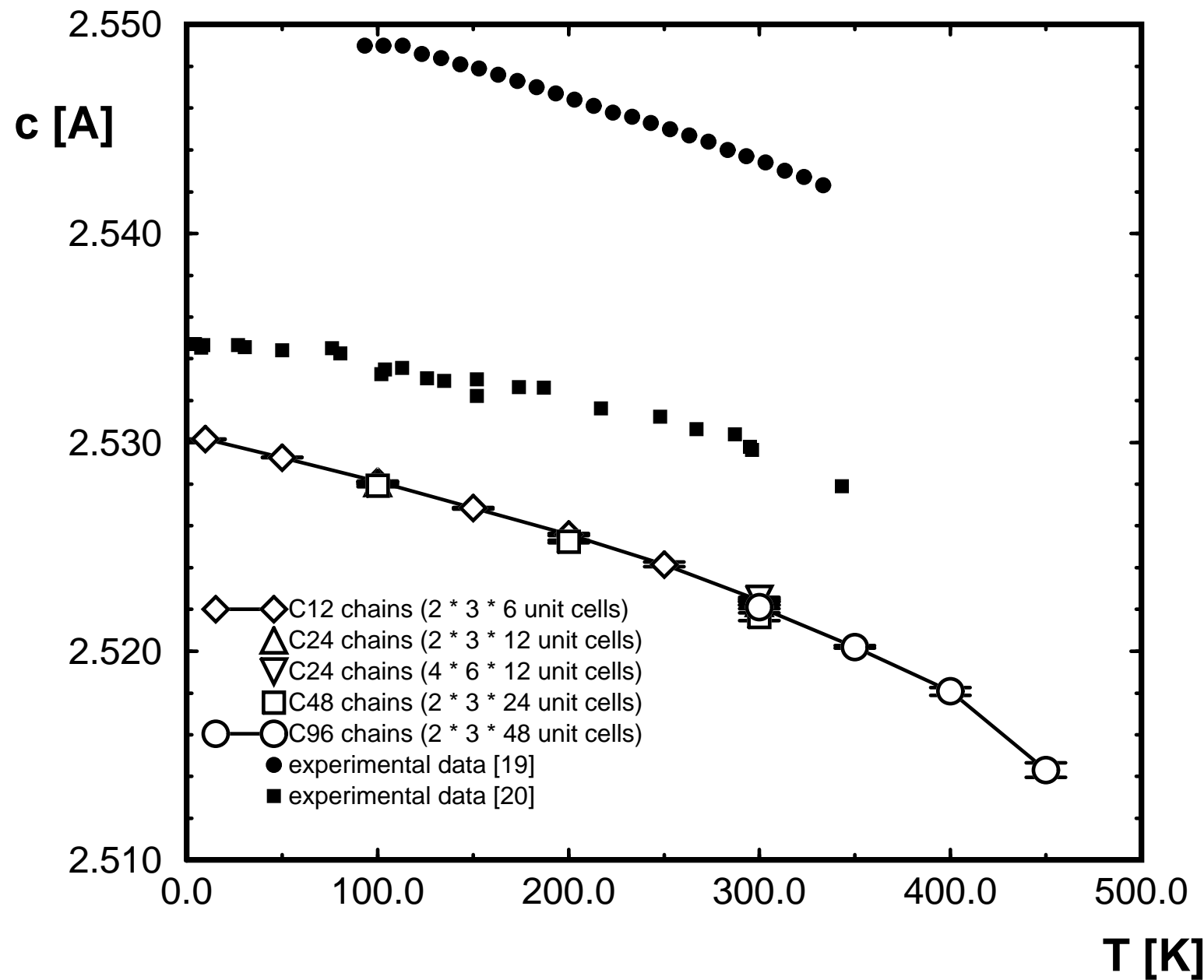


Fig. 4

R. Martonak et al., J. Chem. Phys.

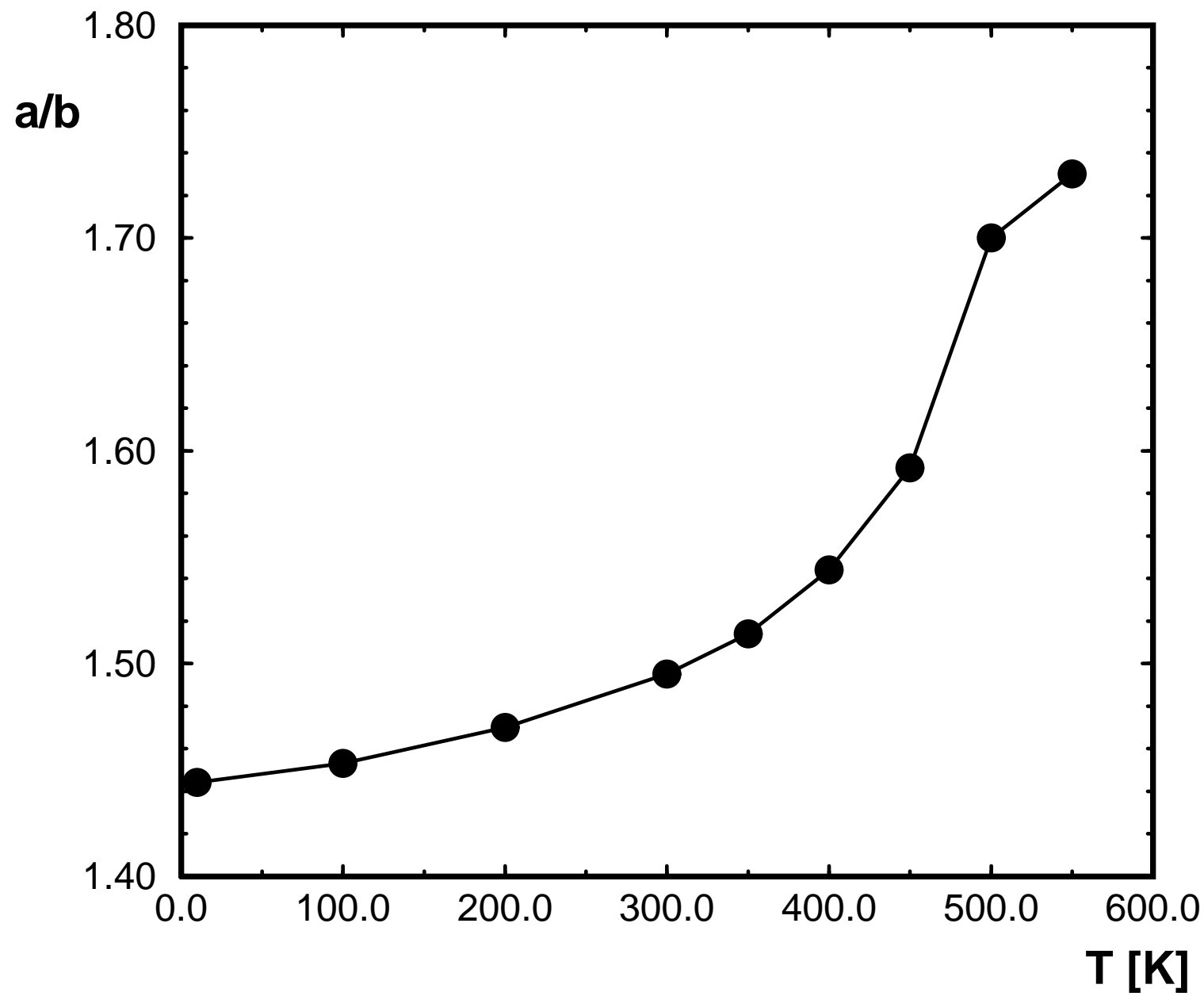


Fig. 5

R. Martonak et al., J. Chem. Phys.

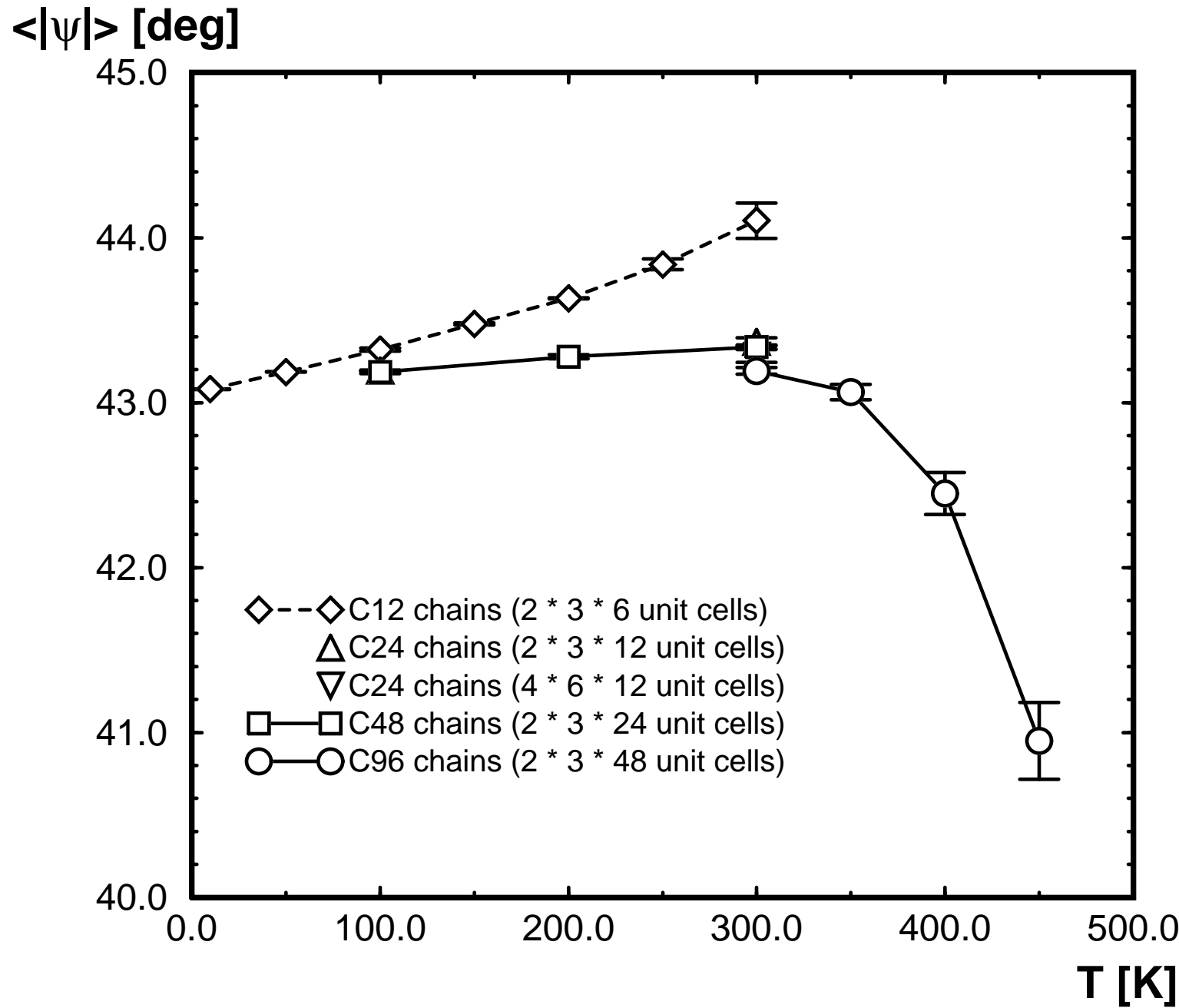


Fig. 6

R. Martonak et al., J. Chem. Phys.

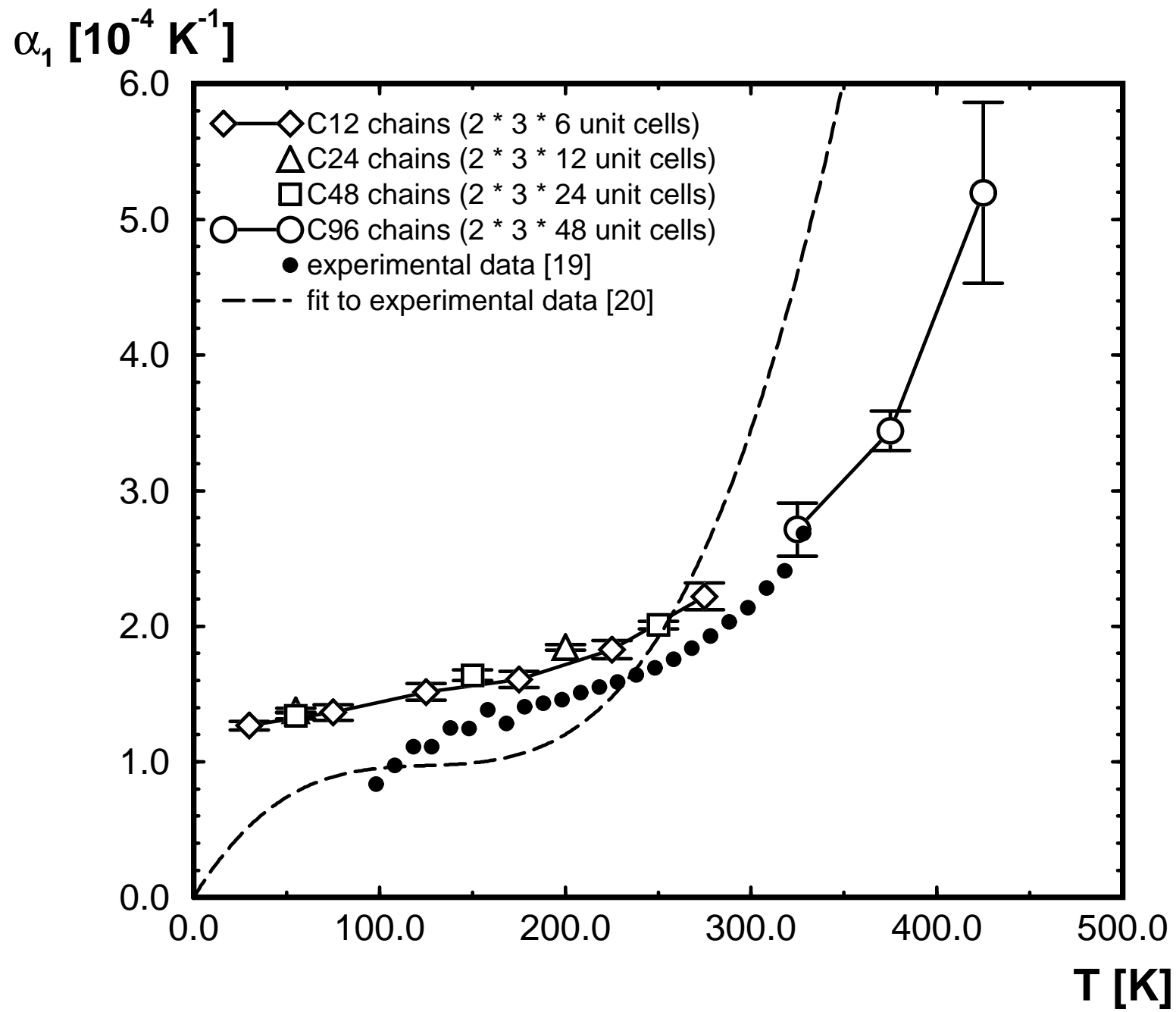


Fig. 7

R. Martonak et al., J. Chem. Phys.

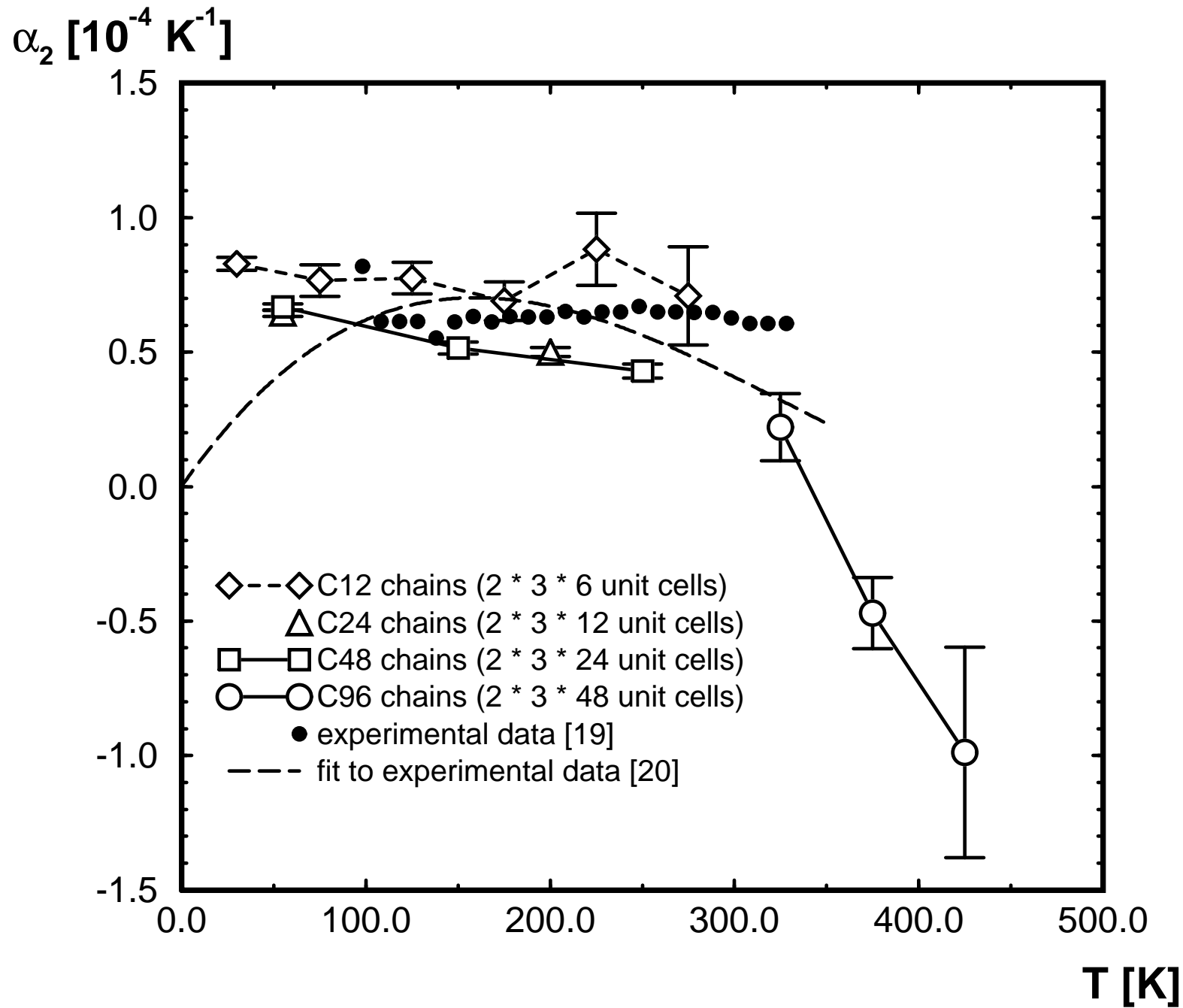


Fig. 8

R. Martonak et al., J. Chem. Phys.

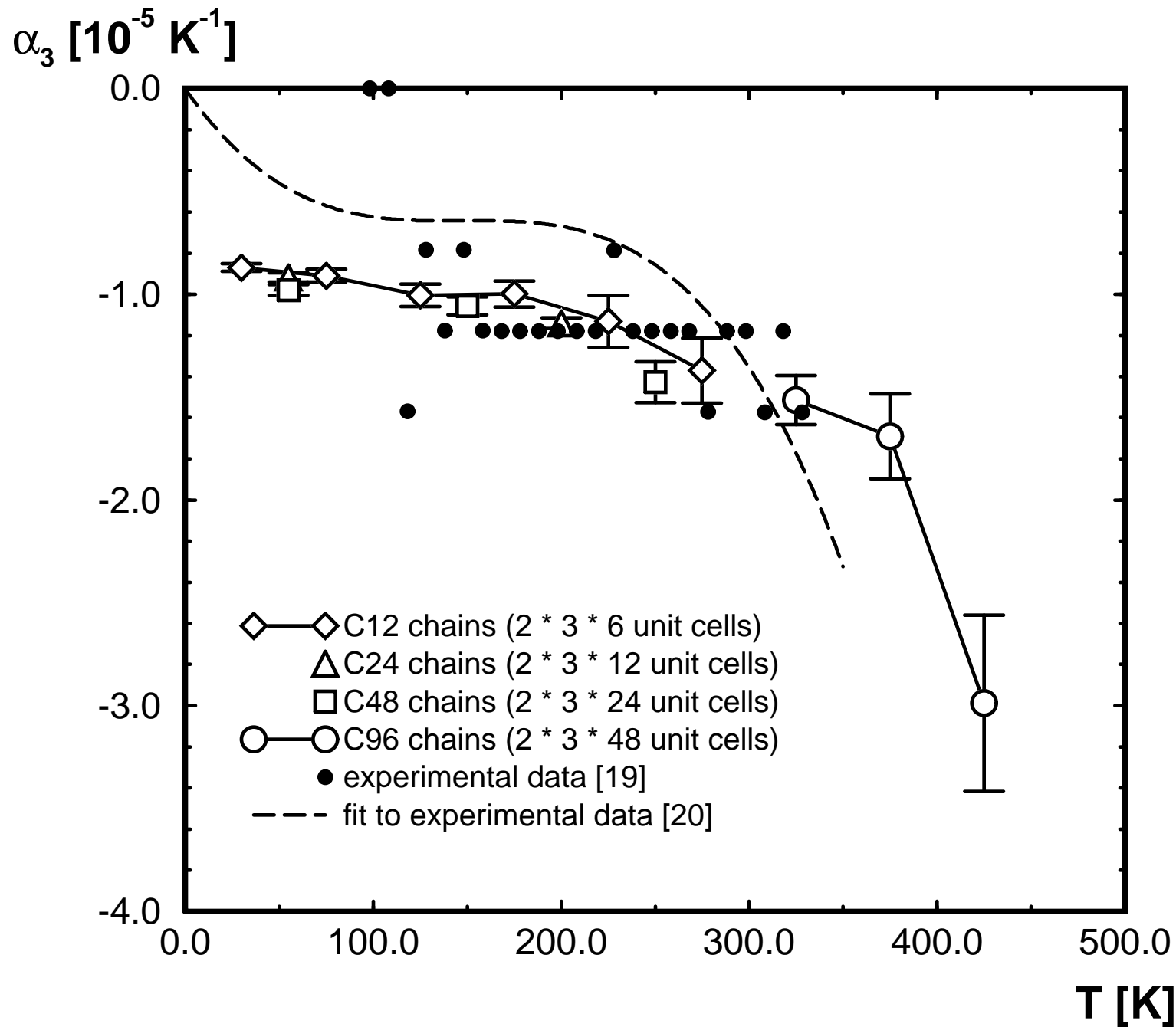


Fig. 9

R. Martonak et al., J. Chem. Phys.

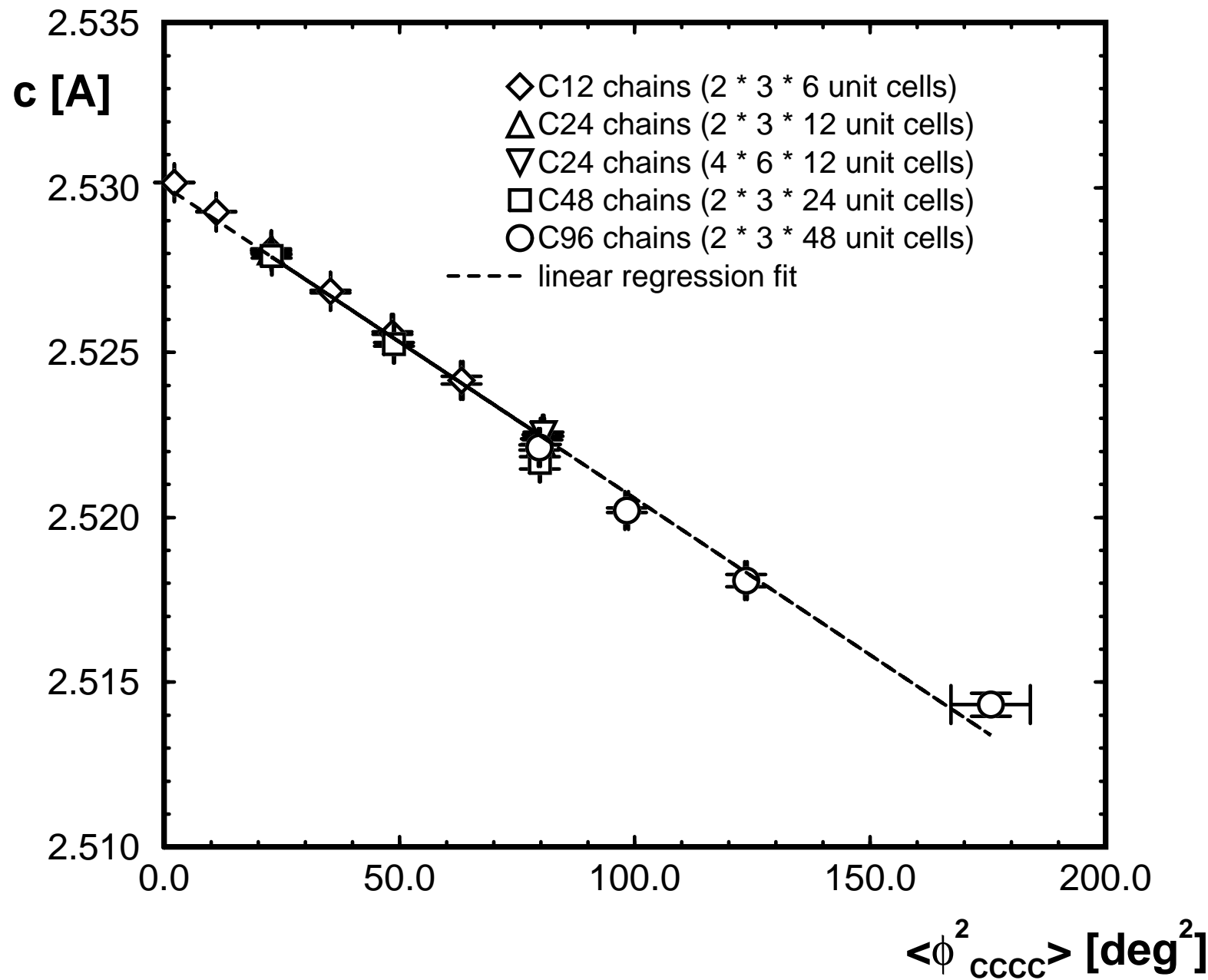


Fig. 10 R. Martonak et al., J. Chem. Phys.

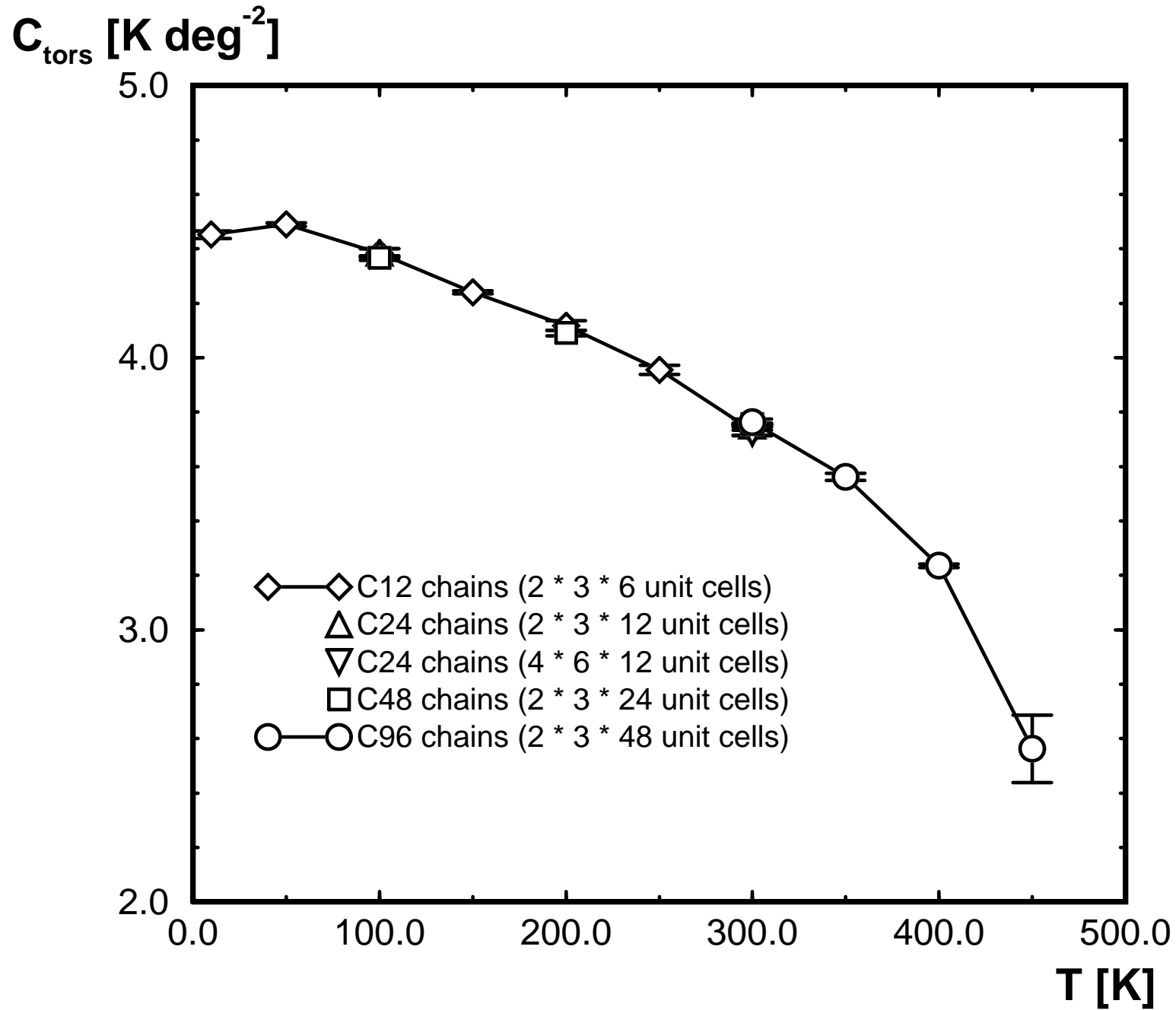


Fig. 11

R. Martonak et al., J. Chem. Phys.

$(\langle (\delta|\psi|)^2 \rangle)^{1/2}$ [deg]

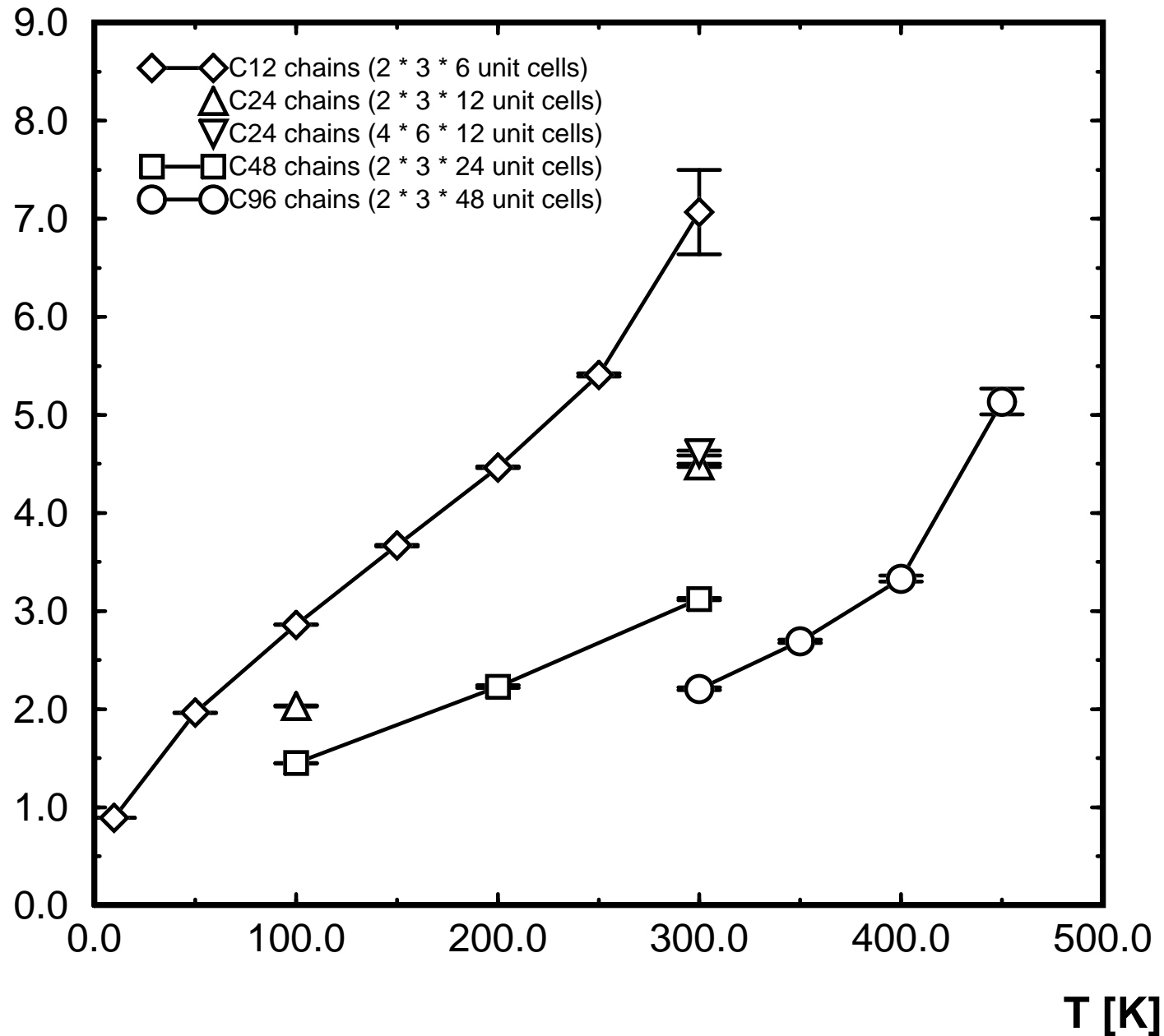


Fig. 12

R. Martonak et al., J. Chem. Phys.

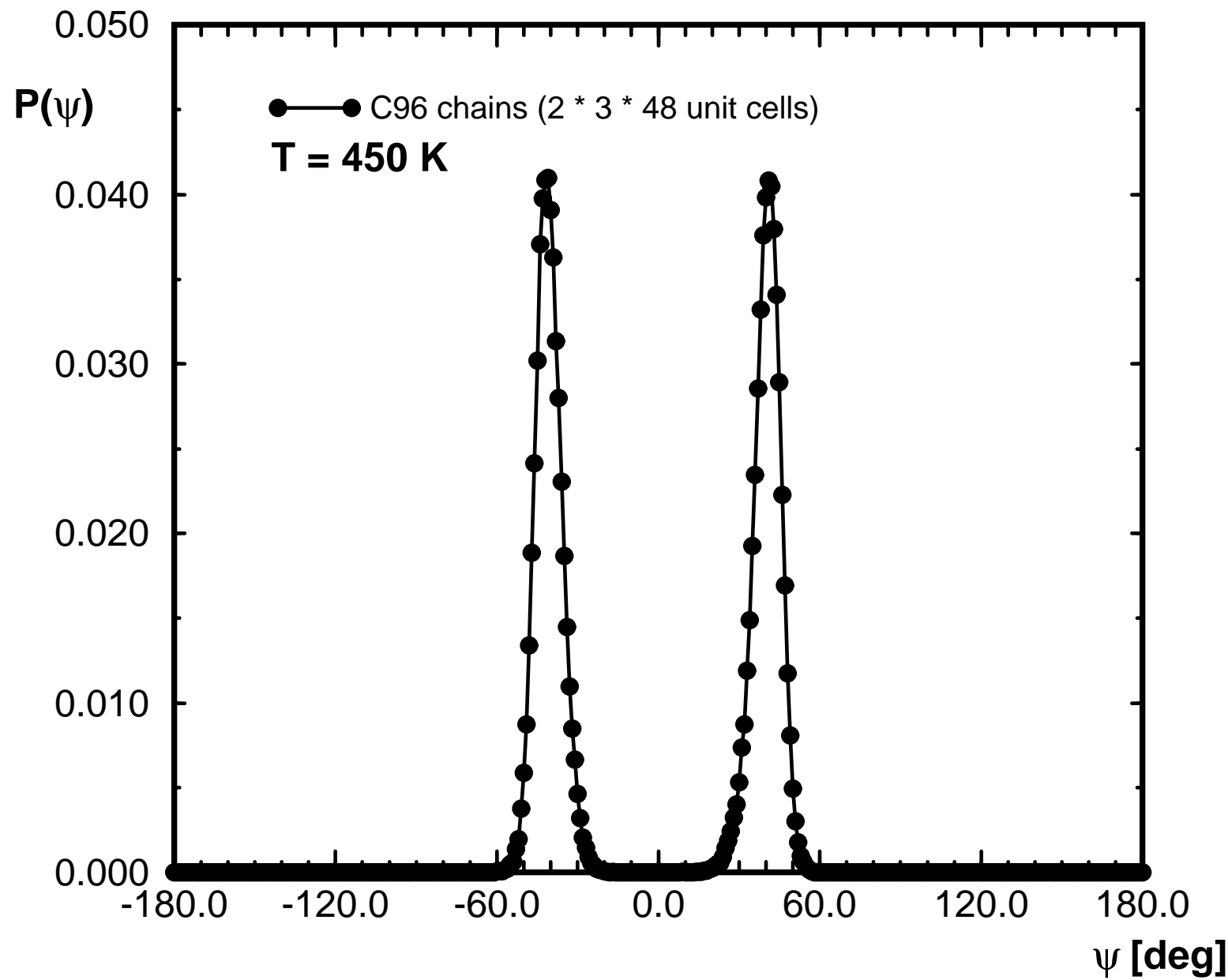


Fig.13 R. Martonak et al., J. Chem. Phys.

$\langle \theta_{ccc} \rangle$ [deg]

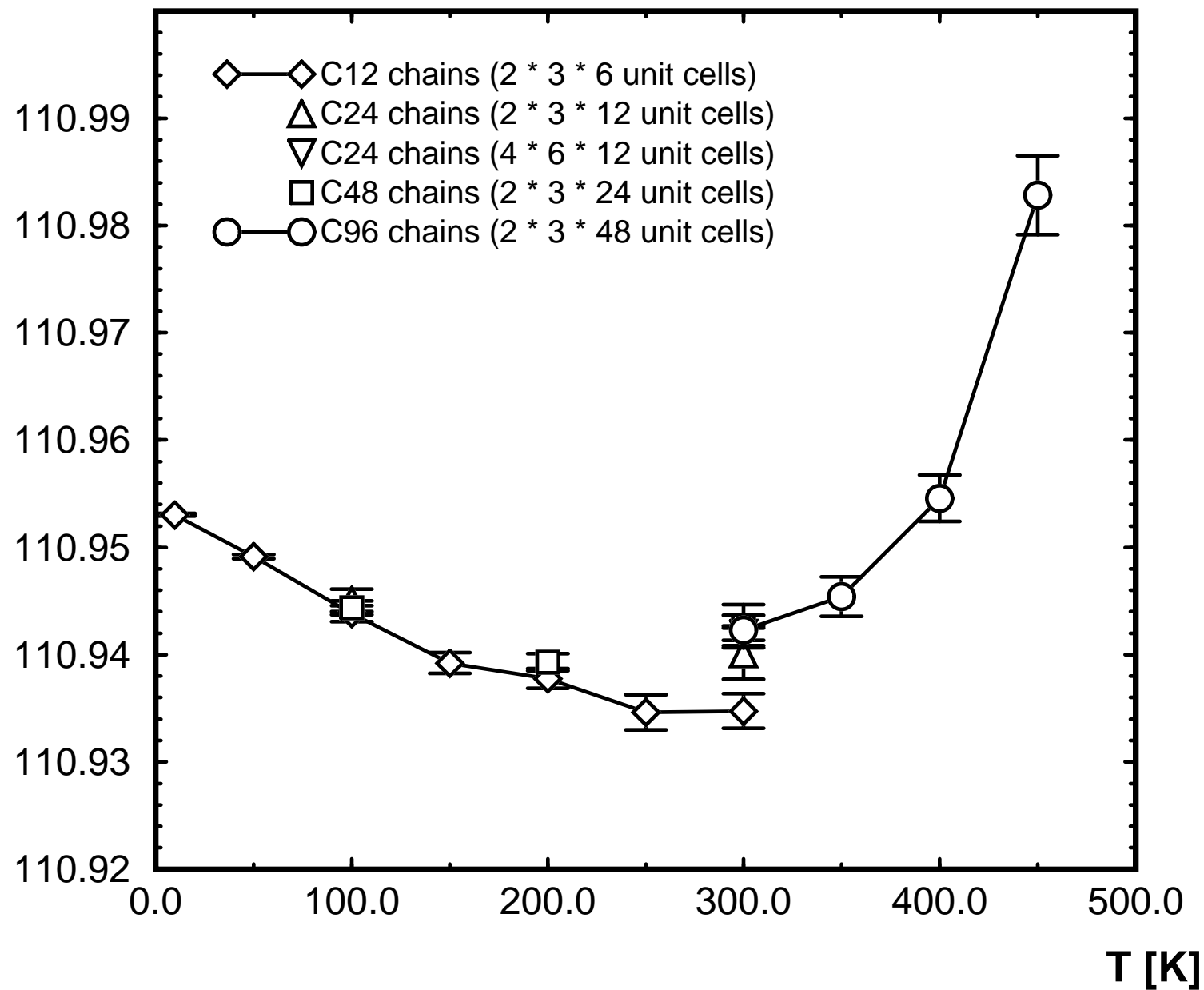


Fig. 14

R. Martonak et al., J. Chem. Phys.

$\langle \theta_{\text{HCH}} \rangle$ [deg]

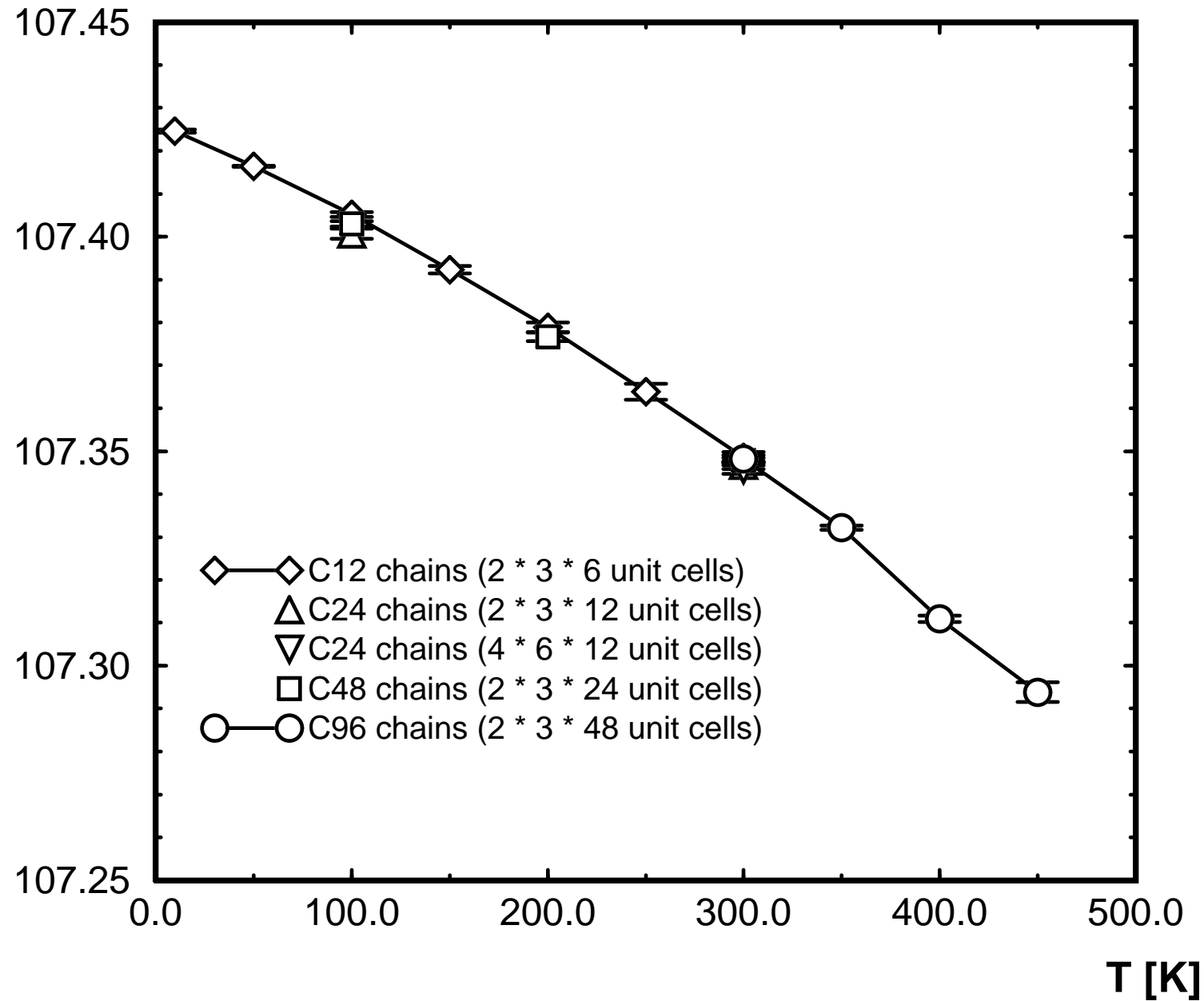


Fig. 15

R. Martonak et al., J. Chem. Phys.

$(\langle \phi_{cccc}^2 \rangle)^{1/2}$ [deg]

15.0

◇ C12 chains (2 * 3 * 6 unit cells)
△ C24 chains (2 * 3 * 12 unit cells)
▽ C24 chains (4 * 6 * 12 unit cells)
□ C48 chains (2 * 3 * 24 unit cells)
○ C96 chains (2 * 3 * 48 unit cells)

10.0

5.0

0.0

0.0

100.0

200.0

300.0

400.0

500.0

T [K]

Fig. 16

R. Martonak et al., J. Chem. Phys.

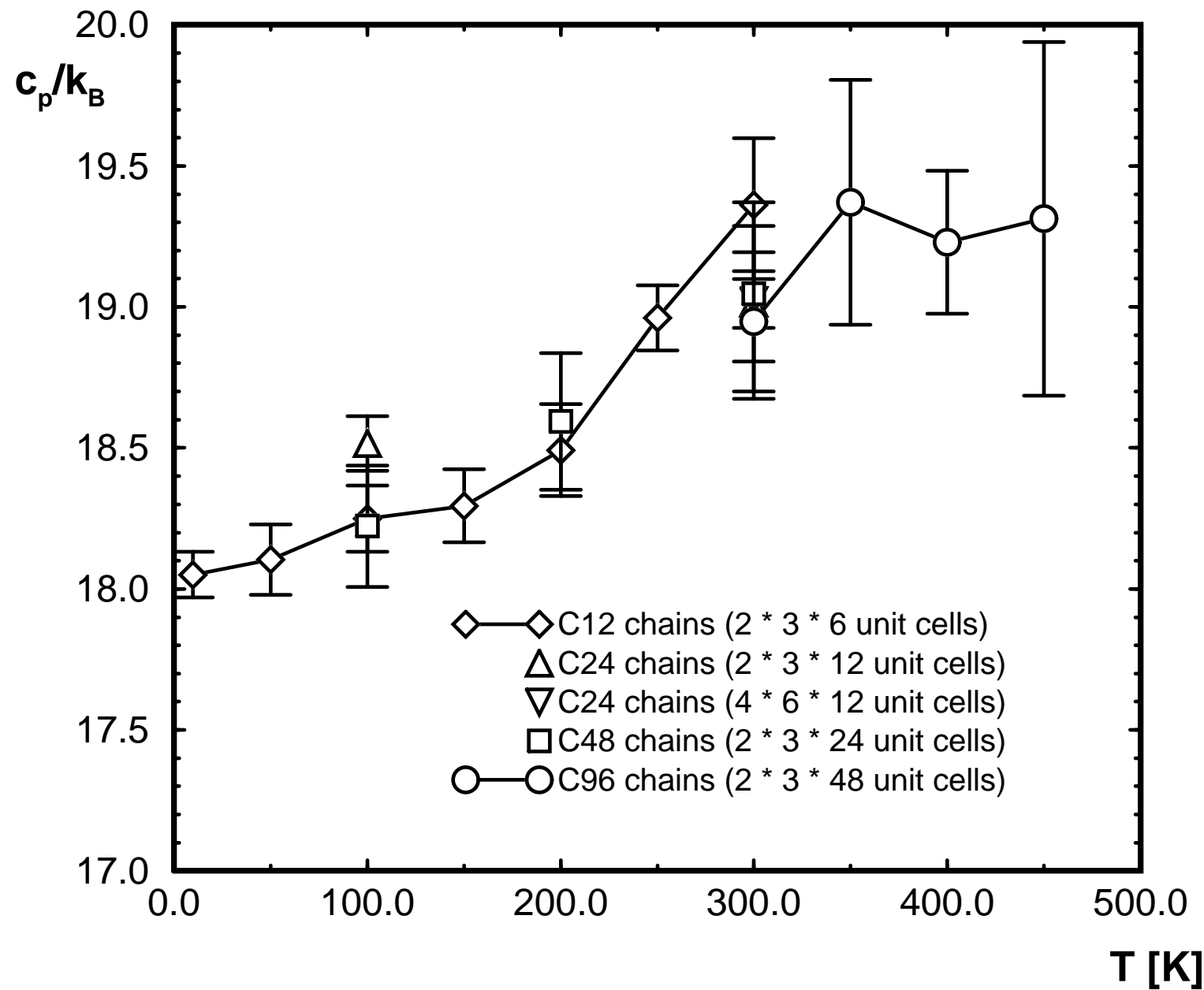


Fig. 17

R. Martonak et al., J. Chem. Phys.

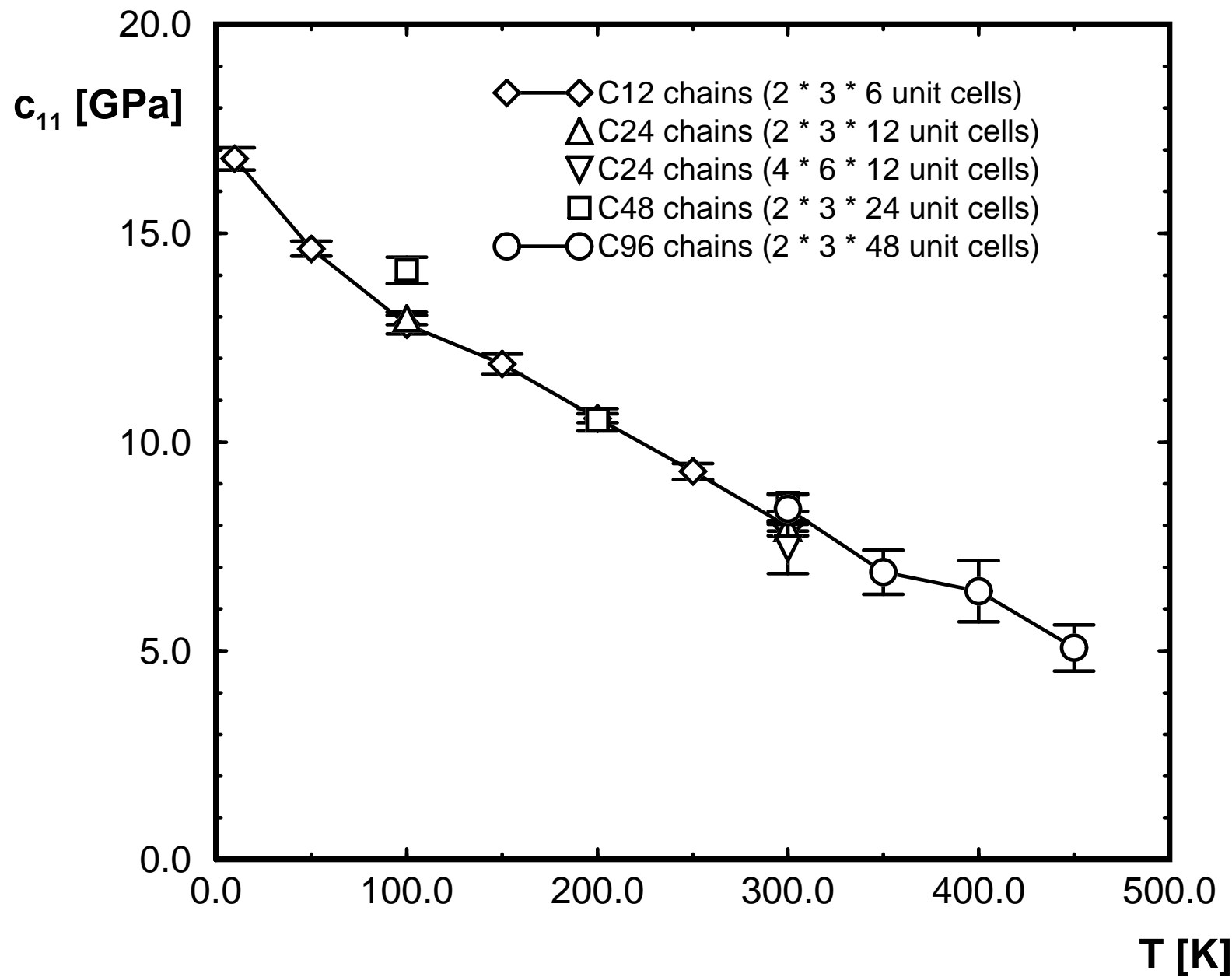


Fig. 18

R. Martonak et al., J. Chem. Phys.

c_{22} [GPa]

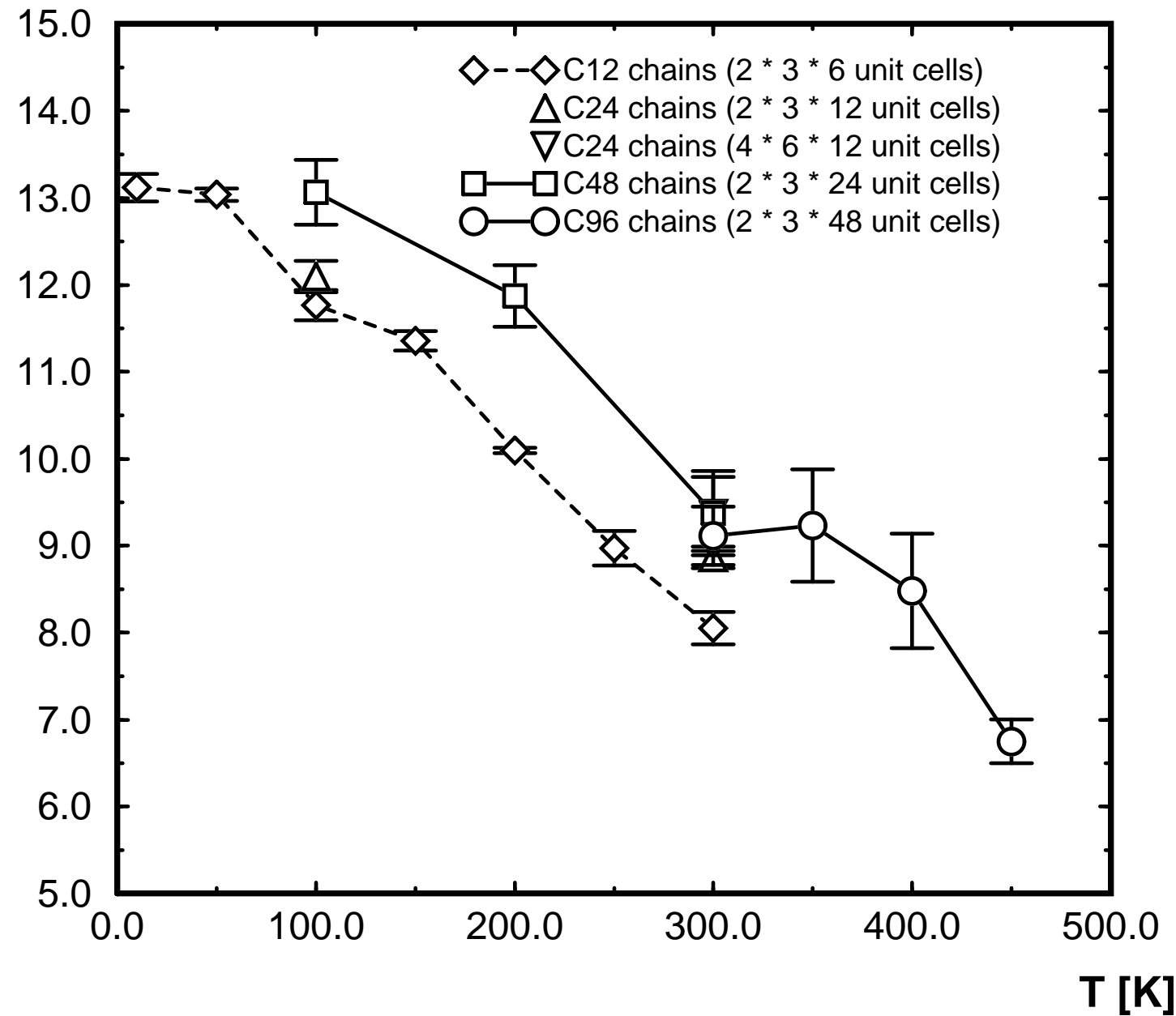


Fig. 19

R. Martonak et al., J. Chem. Phys.

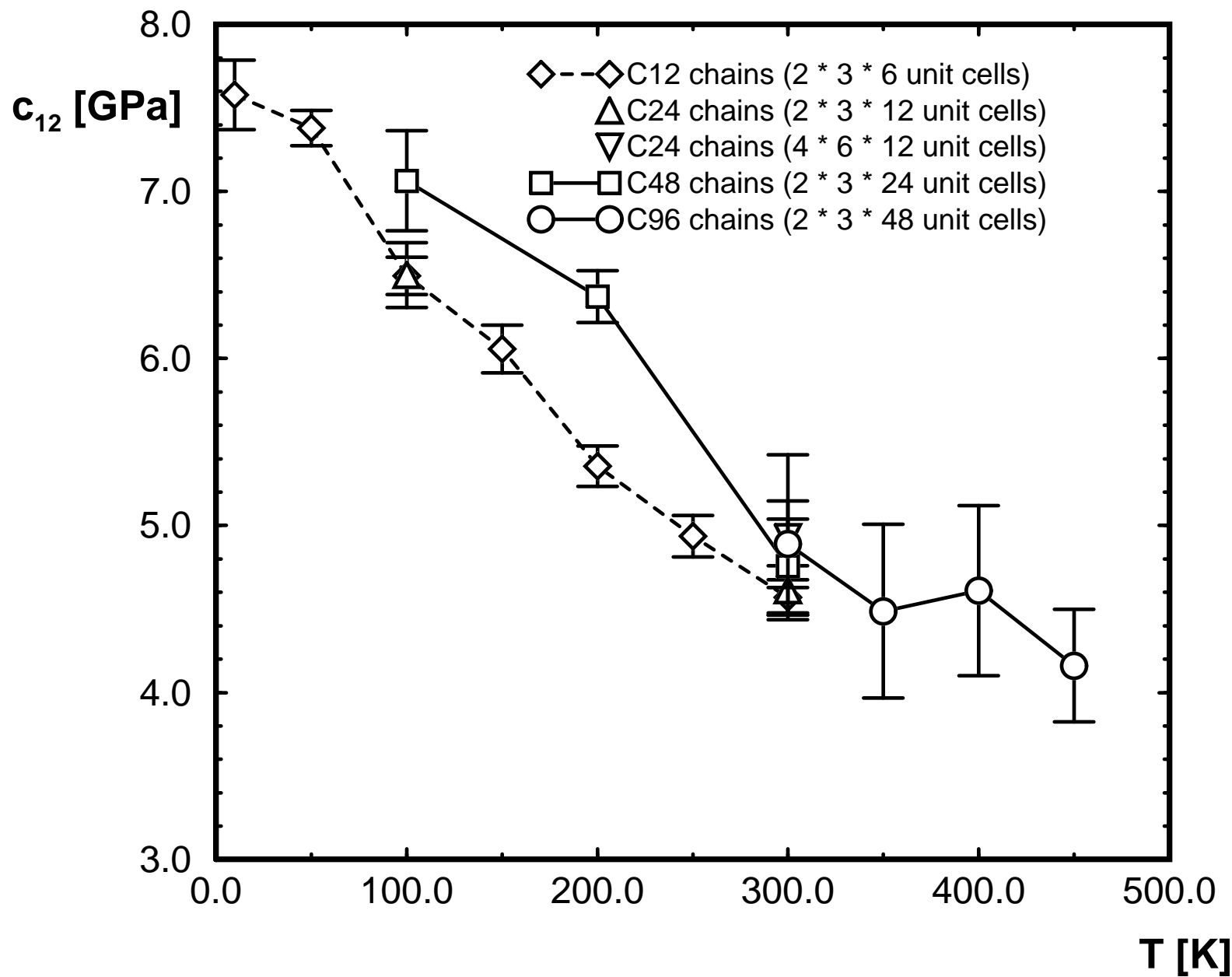


Fig. 20

R. Martonak et al., J. Chem. Phys.

c_{13} [GPa]

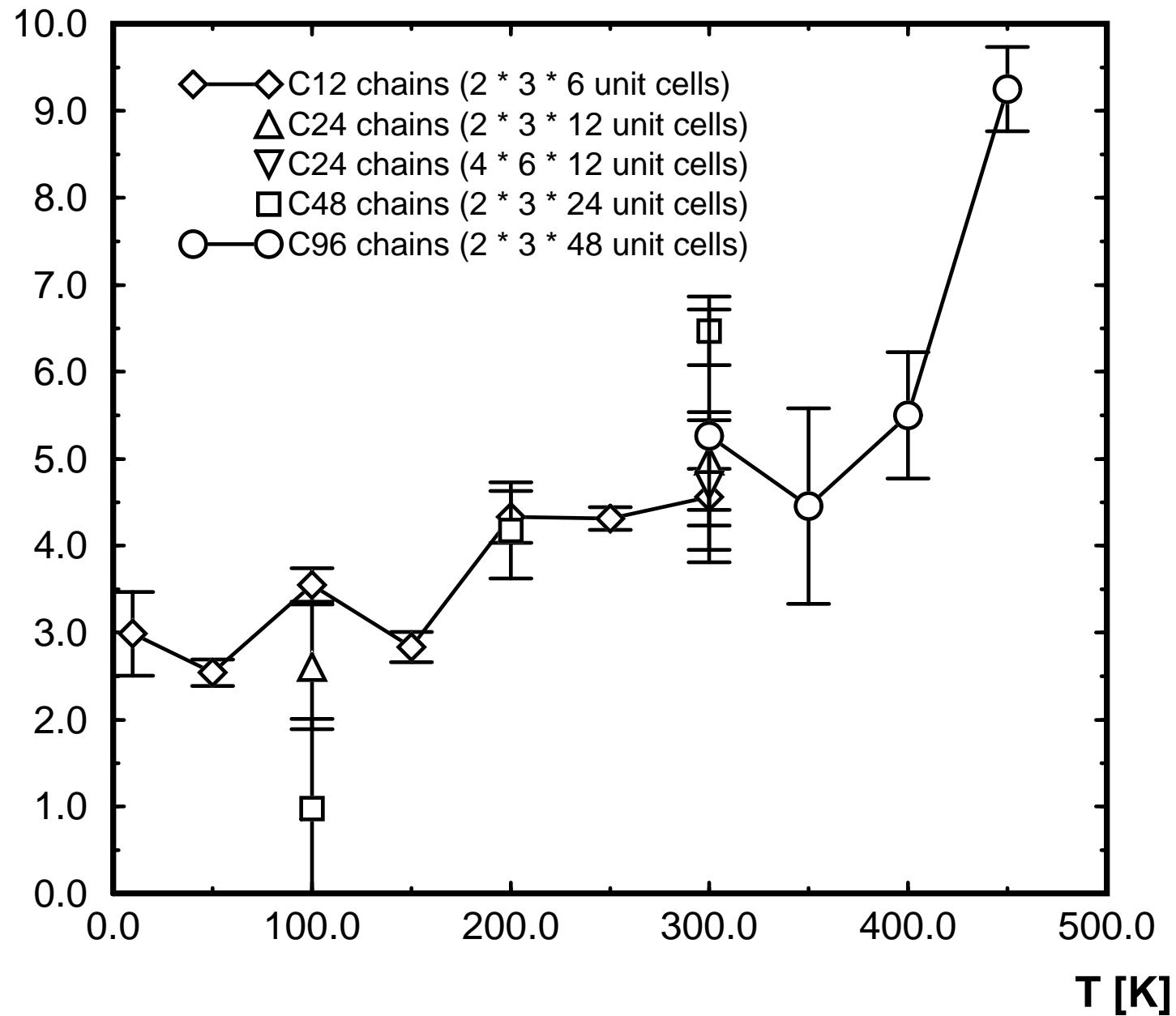


Fig. 21

R. Martonak et al., J. Chem. Phys.

c_{23} [GPa]

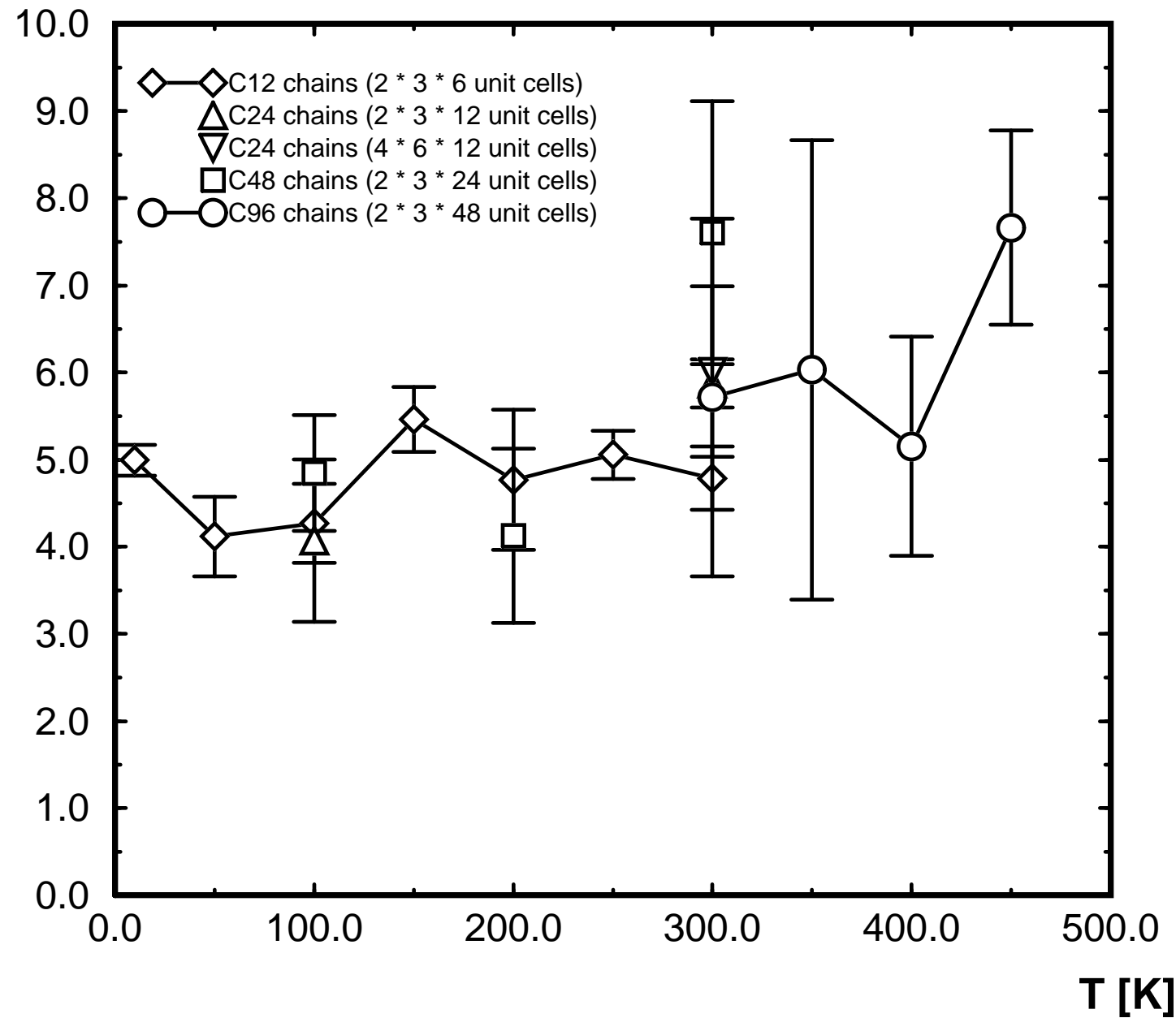


Fig. 22

R. Martonak et al., J. Chem. Phys.

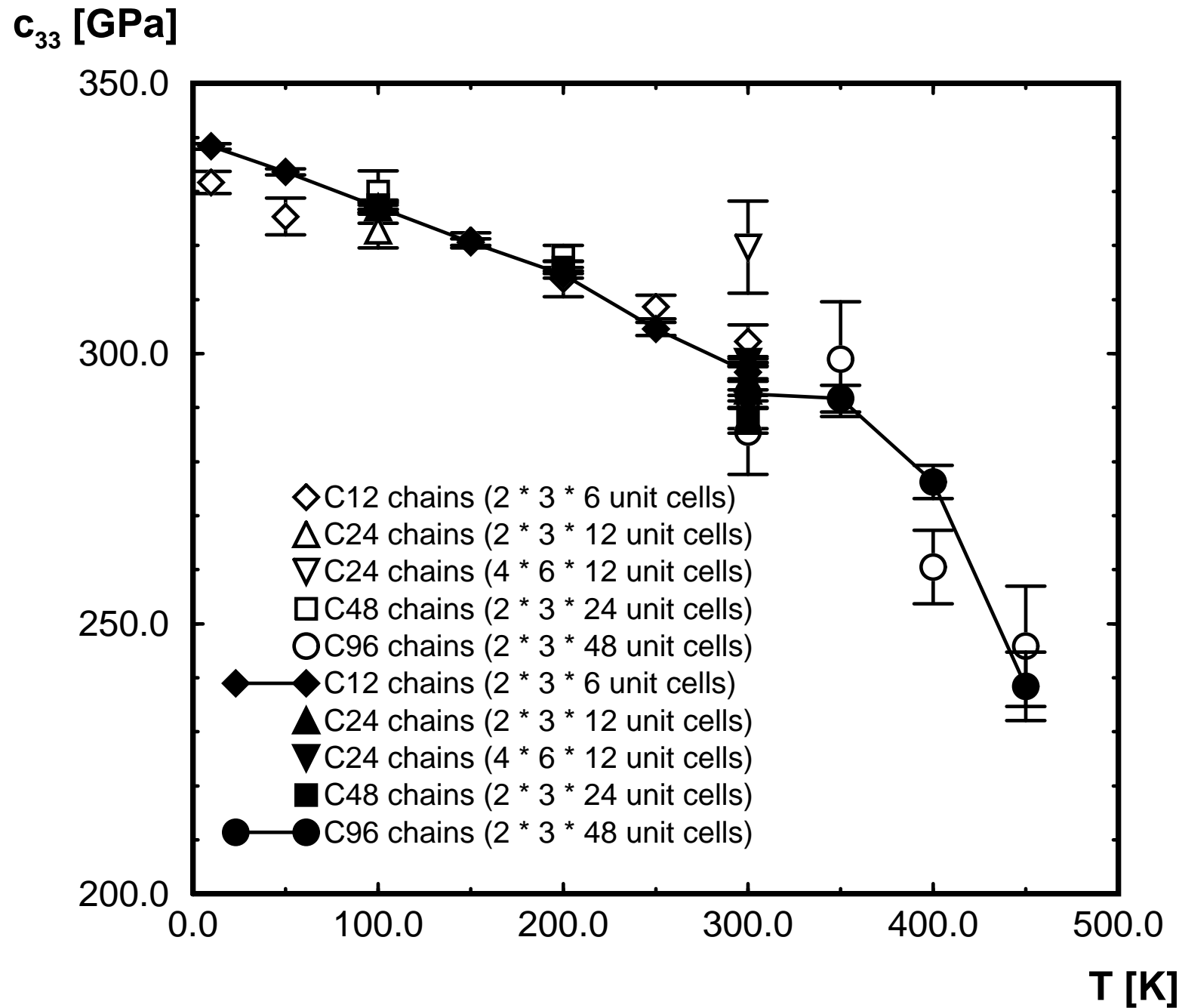


Fig. 23

R. Martonak et al., J. Chem. Phys.

c_{33} [GPa]

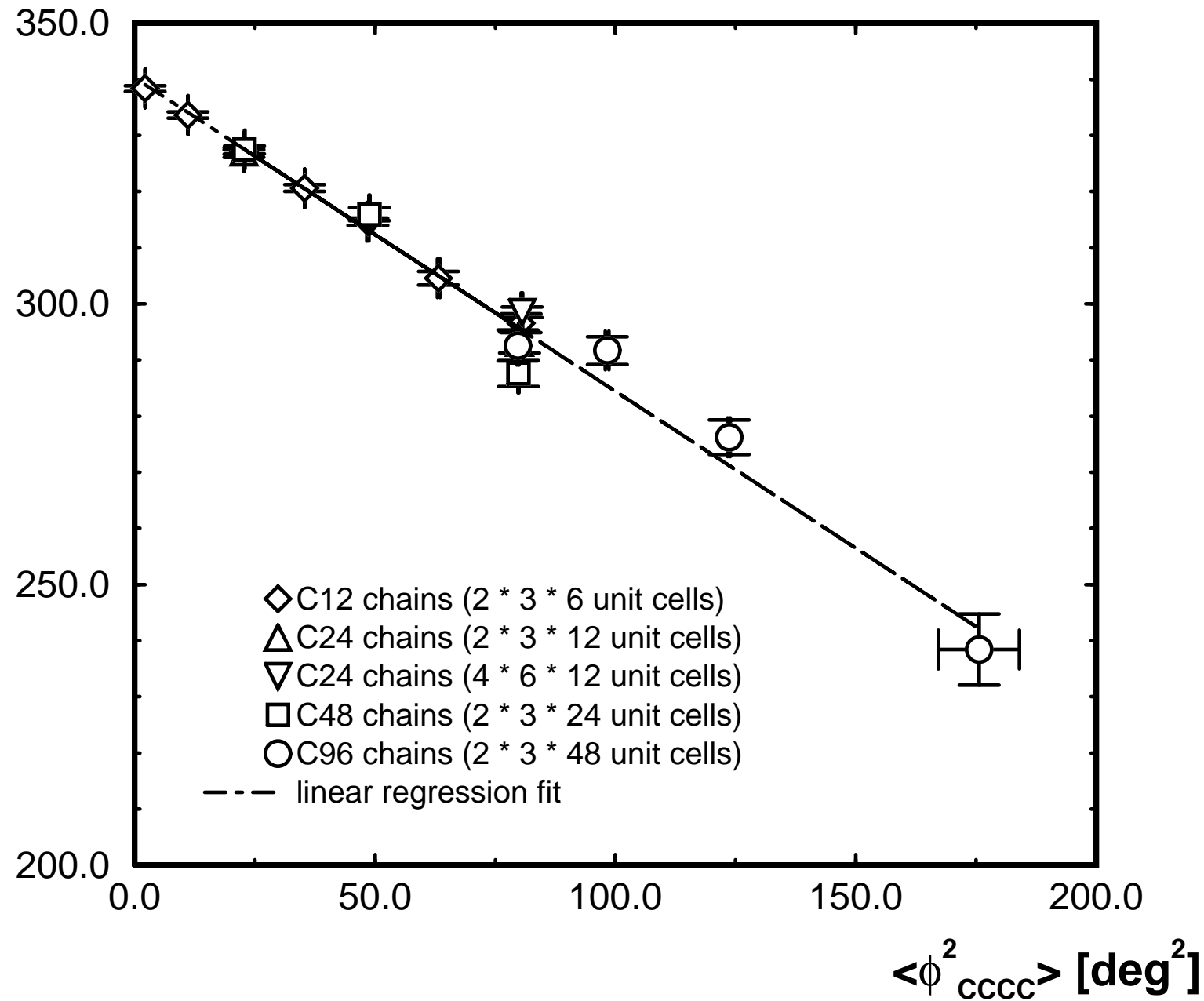


Fig. 24 R. Martonak et al., J. Chem. Phys.